9-1-2008

On the determination of the elastic properties of geopolymeric materials using non-destructive ultrasonic techniques

Joseph L. Lawson

On the Determination of the Elastic Properties of Geopolymeric Materials Using Non-Destructive Ultrasonic Techniques.

by

Joseph L. Lawson

A thesis submitted in partial fulfillment of the requirements for the degree of Master of Science in Mechanical Engineering from the Rochester Institute of Technology, Rochester NY.

THESIS RELEASE PERMISSION
ROCHESTER INSTITUTE OF TECHNOLOGY
DEPARTMENT OF MECHANICAL ENGINEERING

Title of Thesis:
On the Determination of the Elastic Properties of Geopolymeric Materials Using Non-Destructive Ultrasonic Techniques.

I, Joseph L. Lawson, hereby grant permission to Wallace Memorial Library of R.I.T. to reproduce my thesis in whole or in part. Any reproduction will not be for commercial use or for profit.

Signature:_____

Date

ROCHESTER INSTITUTE OF TECHNOLOGY
DEPARTMENT OF MECHANICAL ENGINEERING
ROCHESTER, NY

CERTIFICATE OF APPROVAL

MASTERS OF SCIENCE DEGREE DEFENCE

The Masters of Science Degree Dissertation for
Joseph L. Lawson has been examined and
approved by the thesis committee as satisfactory
for the defense required for the Masters of
Science Degree in Mechanical Engineering

Dr. B. Varela, Advisor Date

Dr. A. Teixeira-Pinto, Co-Advisor Date

Dr. M. Helguera Date

Dr. E. Hensel Date

Dr. H. Gohneim Date

On the Determination of the Elastic Properties of Geopolymeric Materials Using Non-Destructive Ultrasonic Techniques.

by

Joseph L. Lawson

A thesis submitted in partial fulfillment of the requirements for the degree of Master of Science in Mechanical Engineering from the Rochester Institute of Technology, Rochester NY.

Abstract:

Current methods of determining the elastic modulus and Poisson's ratio for geopolymeric materials are limited by the destructive nature of compressive strength and bending testing analysis techniques. Since these tests are not repeatable, there is no means of evaluating whether measured properties are a result of the actual materials or the effect of possible mechanical defects. This study applies a relationship between the speed of sound through a material and its elastic properties to determine the elastic modulus and Poisson's ratio of geopolymeric samples. In addition to these elastic properties, the density, percent pore volume, average pore diameter and standard deviation of pore diameter were also evaluated. These material characteristics were determined as a relationship to the Si:Al ratio of sodium activated metakaolin based geopolymers with Si:Al ranging from 1.49 to 6.4. It was found that lower Si:Al values were consistently around 8.5 GPA while the elastic modulus experienced a decrease to around 5.5 GPa in samples above 3.1 Si:Al ratio. The Poisson's ratio for each sample dereased proportionally to the Si:Al ratio with a maximum value of 0.22 and a minimum value of 0.05.

Acknowledgements:

I have had the pleasure of experiencing amazing support and guidance from many people while pursuing this thesis. I would like to take a moment to thank Dr. Maria Helguera and Raj Panandiker who helped me with the imaging science aspects of my research as well as the development of the testing fixtures. I would also like to thank the shop machinists Dave Hathaway, Rob Kraynik, and Steve Kosciol who were an unbelievable resource throughout my research. I would also like to especially thank my advisor, Dr. Varela. His advice and guidance helped me to author two publications in addition to this thesis as well as complete RIT's dual degree program ahead of schedule. Most importantly however, I would like to thank my new wife, Steph, who was my biggest supporter and greatest friend during this entire process.

Contents

List of Figures

List of Tables

Chapter 1

Introduction

Geopolymers have potential to be a very useful engineering material for a wide range of applications. This class of materials was originally developed in France in the 1980's as the result of a search to develop new fire resistant building materials. Since that time, geopolymers have proven to be effective in any application where ceramics and concretes are currently being used [1]. In order to effectively apply geopolymers as an engineering material, it is essential to understand these materials by quantitatively knowing what their mechanical properties are. Therefore, numerous studies have been conducted over the last three decades to determine how the elastic properties, microstructures, chemical compositions, and curing regiments are related to each other in an effort to tailor geopolymers for specific applications. These studies often report conflicting results and reevaluations are typically impossible because of the destructive nature of most common tests. Therefore it is currently impossible to adequately evaluate the elastic properties of geopolymers while ruling out the possibility of early failures due to structural defects.

The objective of this research is to use non-destructive techniques to determine the elastic properties, namely the elastic modulus and Poisson's ratio, for geopolymers. Ultrasound was chosen as the principal method of investigating the elastic properties of these materials. Ultrasonic testing is not a new technique, it has been thoroughly developed and tested in laboratory and

industrial settings and several ASTM standards have been developed for a large array of testing purposes including locating of cracks and voids, evaluating the effectiveness of ceramic membranes, determining the size and shape of structures that may be hidden from view, and determining the elastic properties of a material. While these methods are reliable and have proven effective in all of these past situations, the use of ultrasound to specifically study the elastic properties of geopolymers is state of the art.

When developing geopolymer materials, there are numerous possibilities and variations that can affect the composition and properties of the material. Chemical compositions, heat treatment procedures, and use of aggregates are a few of the many variables that are concurrently being explored in research around the world. This study in particular focuses on the influence of Si:Al ratios of metakaolin based geopolymers on the elastic modulus and Poisson's ratio of geopolymers. Using chemical compositions that vary only in concentrations of silicon and aluminum, samples with Si:Al ratios ranging from 1.49 to 6.4 were developed and characterized. In order to fully characterize these samples several objectives must be met to determine the properties of the geopolymers as well as evaluate the effectiveness of all tests performed. Specifically, this study aims to investigate the following objectives:

1) Develop an automated ultrasonic testing platform capable of suiting the investigations of this study as well as those of other studies to be conducted through the Multimodal Imaging Laboratory in the Chester F. Carlson Center for Imaging Studies. This apparatus must be designed, built, aligned, and then tested to determine its accuracy and precision.

2) Develop a method for producing geopolymeric samples in a consistent manner over a range of Si:Al ratios from around 1.4 to 6.5. These samples must be created and then finished so that they are applicable to all ASTM guidelines for ultrasonic testing.

3) Determine the speed of sound of longitudinal and shear ultrasonic waves through every geopolymeric sample.

4) Determine the porosity characteristics of each sample using a non-destructive technique. In particular, the percent pore volume, average pore diameter, and standard deviation of pore diameters should be characterized.

5) Determine the density of each sample including the influence of porosities on the densities.

6) Using the density and speed of sound measurements specified above, evaluate the elastic modulus and Poisson's ratio for each sample as a relationship to the Si:Al ratio.

7) Investigate the infrared absorption spectra for each sample to determine the characteristic structures of the geopolymer at each Si:Al ratio. This will help determine the effectiveness with which geopolymerization occurred in each sample.

Chapter 2

Literature Review

2.1 Geopolymer

2.1.1 Geopolymer Terminology

In order to discuss the molecular structures of geopolymers, the term polysialate was coined as a descriptor of the silico-aluminate structure of this type of material, Sialate being an abbreviation for silicon-oxo-aluminate. The tetrahedral molecules, SiO_4 and AlO_4, are linked in an alternating fashion sharing apical oxygen atoms to compose the sialate network which has often been described to be similar to a sodalite network. Due to the negative charge of the Al^{3+} in IV-fold coordination, positive ions must be present to balance out this charge. Generally, either potassium (K^+) or sodium (Na^+) ions are chosen for this reaction, however, other ions such as lithium (Li^+), calcium (Ca^+), barium (Ba^+), ammonium(NH_4^+), and hydronium (H_3O^+) have been used as well [1].

The patterns in which the alumina and silica combine to form the geopolymer binder have also been cited to cause differences in properties and naming conventions have been adapted to describe the possible combinations. While Al-O-Al linkages have been shown to be possible in high energy disordered systems, the nature of geopolymerization makes such linkages unlikely [2]. Therefore, Loewenstien's aluminum avoidance principle, which states that aluminum cannot be bonded together by an oxygen, is generally

accepted when modeling geopolymeric materials because Al-O-Al bonding is more energetically unfavorable [3]. It has been shown that Al-O-Al bonding occurs in metakaolin based geopolymers activated with Na, however, this has only been shown to occur at low Si:Al ratios at or below 1.15 and represent a very small proportion of the bonding structure [4]. Neglecting Al-O-Al bonding the remaining possible bonding combinations allowed are Si-O-Si and Si-O-Al. Based on the chemical combinations of these molecules the designations poly(sialate), poly(sialate-siloxo) and poly(sialate-disiloxo) were defined. These three structures, outlined in Table 2.1 along with their abbreviations, indicate an increasing occurrence of silica-silica bonding when going from PS to PSDS [1].

Table 2.1: Davidovits's proposed geopolymer designations [1]

Name	Abbreviation	Chemical Structure
Poly(Sialate)	PS	(-Si-O-Al-O)
Poly(Sialate-siloxo)	PSS	(-Si-O-Al-O-Si-O)
Poly(sialate-disiloxo)	PSDS	(-Si-O-Al-O-Si-O-Si-O)

2.1.2 Geopolymerization

Aluminosilicate materials containing aluminum in IV-Fold coordination are necessary for the alkali activating process of geopolymerization. Should other coordinations of aluminum be present in the source materials for geopolymerization, the IV-fold aluminum will dominate the reaction and will be completely exhausted while aluminum (V) and aluminum (VI) remain unreacted unless converted to the less stable formation [5]. Aluminosilicates that are

naturally occurring in the crust of the earth are the main sources of these materials, namely kaolinite, feldspars, mine tailings, volcanic ashes, as well as numerous other forms of minerals and clays [6]. Other sources of materials that are rich in aluminum and silicon which can be used for geopolymerization include byproducts of industrial processes such as fly ash, which is the waste product of coal combustion plants, furnace slag, and construction residuals [6].

The process for the formation of the aluminum and silicon in IV-Fold coordination typically follows one of two chemical processes. The most commonly applied method of obtaining these materials involves calcining aluminosilicate hydroxides such as kaolinite according to the reaction listed below [1].

$$Si_2Al_2O_5(OH)_4 \rightarrow Al_2Si_2O_7 + 2H_2O$$

Studies have shown that the above process requires up to 750 °C and can complete itself in only two hours [7]. The geopolymerization process itself is an exothermic polycondensation reaction involving alkali activation by a cation in solution. The reaction leading to the formation of a polysialate geopolymer is described below [1]:

$$(Al_2Si_2O_7)_n + nH_2O \xrightarrow{MOH} n(OH)_3 - Si - O - Al - (OH)_3$$

$$n(OH)_3 - Si - O - Al - (OH)_3 \xrightarrow{MOH} M\left(- \underset{\underset{O}{|}}{Si} - O - \underset{\underset{O}{|}}{Al^{(-)}} - O \right)_n + nH_2O$$

Where M is the cation used to activate the reaction which is typically introduced as either potassium hydroxide or sodium hydroxide. Additional amounts of amorphous silica must be present in order to form either the polysialate-siloxo or polysialate-disiloxo structures of geopolymers. The reaction for the polysialate-siloxo formation is also provided as an illustration of how the two reactions differ [1].

$$\left(Al_2Si_2O_7\right)_n + nSiO_2 + nH_2O \xrightarrow{MOH} n\left(OH\right)_3 - Si - O - \underset{\left(OH\right)_2}{\overset{(-)}{Al}} - O - Si - \left(OH\right)_3$$

$$n\left(OH\right)_3 - Si - O - \underset{\left(OH\right)_2}{\overset{(-)}{Al}} - O - Si - \left(OH\right)_3 \xrightarrow{MOH} M\left(\begin{array}{ccc} | & | & | \\ -Si-O-Al^{(-)}-O-Si-O \\ | & | & | \\ O & O & O \end{array} \right)_n + nH_2O$$

After the process is completed the final geopolymer can be described by the empirical formula:

$$M_n\{-(SiO_2)_z-(AlO_2)\}_n + H20$$

Where, again, M is a cation used to activate the reaction, n is the degree of polycondensation, and z = 1,2,3 for polysialate, polysialate-siloxo, and polysialate-disiloxo structures respectively [1].

2.1.3 Geopolymer Properties

In order to use geopolymers as an engineering material, knowledge of their physical properties must be fully understood. While the earliest of this research was conducted through industry and kept as proprietary knowledge [1] there have been numerous studies within the last three decades attempting to classify this material.

Geopolymers have often been explained in terms of their microstructural properties. This includes both the porosity of a sample and extent to which the geopolymerization takes place. Using nuclear magnetic resonance a presence of aqueous $Al(OH)_4^-$ was discovered to be trapped inside pores within the geopolymer binder [5]. This implies that not only is a portion of the aluminum not being reacted, but this inability to completely react creates porosities [5]. The presence of this aqueous phase was also correlated to the silicon to aluminum ratio used to prepare the sample and found that geopolymers with $Si:Al \leq 1.40$ cannot be accurately characterized by their Si:Al ratio because the degree of unreacted aluminum is too great [5]. In fact, when curing conditions and source materials are held constant, the Si:Al ratio directly affects the nature of the porosity with higher Si:Al ratios having larger overall pore volumes but lower average pore diameter [8]. This same effect was also analyzed in another study in an attempt to tailor porosity to meet specific properties. It was discovered that

choosing an appropriate alkali activator and curing conditions would enable the ability to control the geopolymerization process and obtain desired porosities [9]. Other studies have also shown that Si:Al ratios directly affect the rate and extent of geopolymerization. It has also been shown that incomplete geopolymerization can lead to pockets of unreacted metakaolin which act as structural point defects within the material [10]. While studying the effect of the chemical composition on this phase, this study determined that increasing the SiO_2:Al_2O_3 ratio will decrease the percent of unreacted metakaolin; however, the unreacted phase was still present even with SiO_2:Al_2O_3 ratios as high as 15 [10]. Other reports have found that the geopolymerization is carried out more fully as additional silica is added to the sample until an equilibrium point is reached where the excess silica begins to hinder the alkali cations ability to react with the aluminum [11]. It has also been shown that controlling the SiO_2:M_2O ratio will influence reactivity. It was determined that the maximum amount of geopolymerization occurs around SiO_2:M_2O = 2.00 with a decreasing amount of reactivity as SiO_2:M_2O ratios deviate from that point [11]. Still others theorize that the source material itself is responsible for the extent of unreacted materials. It has been discovered that geopolymerization reactions only occur at the surfaces of the particles of source materials [12]. Therefore, the particle size of the source materials will be the main factor in determining the extent of geopolymerization where source materials

with high specific surface area will react more homogeneously due to the higher availability of surface molecules which can interact in the reaction [13].

In order to effectively apply geopolymers as an engineering material, many researchers have sought to determine the mechanical and elastic properties of geopolymers such as Young's modulus, Poisson's ratio, compressive strength, and flexural strength. Typically this is done over a series of samples that are slightly altered in their chemical composition or curing regiment so that a qualitative trend can be applied. Since the properties of geopolymers have been shown to be susceptible to many different variables it is still presumptuous to quantitatively predetermine the values of any such property without testing [14, 15, 16]. In fact, one study investigated the flexural strength as a function of cure regiments for two different fly ash compositions taken from the same coal fired power plant in New Zealand and found different results from each sample set [16]. Therefore, even though the actual values determined by past research may be inapplicable to future work, they are still useful by means of providing an expected order of magnitude of these properties as well as a trend for how they will be affected by chemical changes.

Many studies have been performed to determine the compressive strength and flexural strength of geopolymers. For kaolin based geopolymers without aggregates, the compressive strengths range from 10 MPa to 85 MPa [8, 12, 13,

14, 15, 17] while fly ash based geopolymers without aggregates have been shown to range between 20 MPa and 80 MPa [18]. Flexural strength for metakaolin based geopolymers without the use of aggregates has been measured at values ranging from 6 MPa to 8 MPa [18]. Fly ash based geopolymers without aggregates have been recorded as having a flexural strength ranging from 2.0 MPa to 14.2 MPa [16, 19]. Samples cured at elevated temperatures have been shown to increase in compressive strength when they are heat treated for longer periods of time [19]. There also seems to be a trend for geopolymers to increase in strength as the Si:Al ratio increases up until a point where the excess silica hinders the reaction [8]. When studying metakaolin based geopolymers, 1.90 was found to be the optimal Si:Al ratio for maximum strength [8]. Choice of alkali activator is also important. When metakaolin geopolymers were evaluated over a long period of time, Na activated polymers had a tendency to increase in strength while K activated polymers had the opposite tendency, decreasing in strength [17]. However, the strongest specimen from this study was found to have a combination of Na and K activators [21]. Different additives have also been studied in an attempt to further increase the compressive strength. Some additives, such as Portland cement and lead, have lead to increasing strength [15, 22], while other additives, like inorganic salts, polytetrafluoroethlene (PTFE), graphite and molybdenum(MoS_2), have had a negative impact [14, 20]. The

extreme values found in the literature for both compressive and flexural strength for metakaolin and fly ash based geopolymers are displayed in table 1.1 as an indicator of the typical ranges observed for this type of material.

Table 2.2: Range of compressive and flexural strengths of geopolymer marterials found in state of the art literature.

Source Material	Compressive Strength		Flexural Strength	
	Low	High	Low	High
Kaolin	10 MPa	85 MPa	6 MPa	8 MPa
Fly Ash	20 MPa	80 MPa	2.0 MPa	14.2 MPa

Other than strength, Young's modulus or elastic modulus is the most commonly investigated property of geopolymers for its obvious importance towards engineering applications. Due to the porous nature of geopolymers, complicated fracture mechanics lead to wide ranges of uncertainties when strengths are experimentally evaluated due to the destructive nature of these tests; therefore, it has been suggested that Young's modulus and not the compressive strength is the most effective mean of rating the physical nature of geopolymeric materials [8]. Typical values for Young's modulus reported throughout the literature for metakaolin based geopolymers without aggregates range from 1 GPa to 6 GPa [8, 17]. Similarly to the compressive strength, the Young's modulus tended to increase in value as the Si:Al ratio increased until around Si:Al ≥ 1.65 when it reached an equilibrium point at the maximum value [17]. It has also been hypothesized that this trend is more closely associated with

the homogenization of the microstructure of the material as opposed to the Si:Al ratio [8]. The extreme values found in literature for the elastic modulus of geopolymeric materials are presented in table 2.3 as an approximate range of expected values for geopolymeric materials.

Table 2.3: Typical range of Elastic Modulus values for properties of geopolymers found from literature

Source Material	Low	High
Kaolin	1 GPa	6 GPa

2.1.4 Geopolymer Applications

Cementitious materials with properties such as quick setting, low permeability, acid resistant, high early strength, fire resistant, and low costs have numerous possibilities for industrial applications. The original application of geopolymers was as a fire resistant material [1]. Geopolymers are ideal for high temperature applications because, even though its thermal conductivity increases with temperature, the thermal conductivity still remains lower than that of other structural metals by an order of magnitude or more [3]. Furthermore, while concrete may explodes at temperatures around 450°C, geopolymers have been shown to remain structurally stable at temperatures up to 800°C [3]. When combined with carbon fibers to form a composite material, geopolymers proved to cost less than traditional carbon fiber/resin materials and perform better

without any ignition, burning, or smoking and retain 63% of its initial flexural strength at temperatures where resins loose almost all of their strength [23].

Need for green technologies have also created applications for geopolymers in areas involving immobilizing toxic metals and reducing CO_2 emissions [1]. Producing ordinary Portland cement generates a great deal of CO_2. It has been estimated that for every ton of cement that is produced by traditional methods, approximately one ton of CO_2 is also produced [24]. In order to combat this pollution source, geopolymers have been used either as replacements to or as additives to cement because of the similar nature and properties of these materials [24, 25]. The reduction of energy required to produce geopolymers as compared to Portland cement is also significant; clinker, a component of Portland cement requiring calcination, requires 1450°C whereas, metakaolin can be formed at 750°C over a shorter period of time and fly-ashes do not require any pre-treatment [7]. Geopolymers are also an environmentally friendly material because they can be formed out of waste materials, such as fly ash, furnace slag, or volcanic ash, that typically are discarded [25]. A third environmental application of geopolymers is as a means to immobilize toxic wastes, such as arsenic, mercury, and lead along with other heavy metals, asbestos, and radioactive wastes, some of which are often thrown into landfills where they pose a risk to local bodies of water and agriculture [26]. Geopolymers are an

excellent choice of construction materials whenever landfills and waste sites are being constructed and can be used as a solid basis to prevent leakages and erosions, an effective cap to prevent rain water contamination and provide a safe cover for the purpose of building, and as interior structures to prevent wastes layers from contacting each other or dangerously shifting [26].

2.2 Non-Destructive Ultrasonic Techniques

Ultrasonic techniques have proven to be a very reliable and repeatable method of investigating substances when destructive testing techniques are unaffordable, unreliable, or simply unwanted [27]. It is a valuable tool because of its versatility, capable of being applied not only in the laboratory, but also as a method of inspection in a manufacturing setting and in the field [28].

2.2.1 Ultrasonic Terminology

Ultrasonic waves are created and received by ultrasonic transducers containing a piezoelectric crystal which has the unique property of inducing a voltage whenever the crystal undergoes deformation [29]. Similarly, whenever a voltage is applied to a piezoelectric material, the lattice of the material structure will deform causing it to restructure itself [29]. This means that the piezoelectric crystal in the ultrasonic transducer can generate an acoustic wave as well as

interpret an acoustic signal [29]. When the same transducer both generates an acoustic wave and records the same reflected acoustic wave, it is said to be a pulse-echo test [30]. A test involving two transducers, one of which generates a signal and another which receives the signal, is said to be a transmit-receive test [30]. The transducers involved in a transmit-receive test can either be aligned with each other, offset laterally by a distance, or at differing angles with respect to the test piece depending on the set up of the test and the information which is desired [30]. Ultrasonic transducers commercially available are capable of generating both longitudinal and shear waves [31].

The basic principle of ultrasonic testing applications is that whenever a mechanical wave traveling through a medium encounters change of phase within the material, the wave will either reflect, refract, or diffract [29]. This change of phase is typically caused by a surface of the material, a pore, or a defect [31]. These structures are often simply referred to as scatterers because of the nature of an acoustic wave to scatter or deviate from its path whenever encountering this change [29]. Whenever a sound wave contacts a scatterer within a structure, some of the wave will refract and continue to travel through the scatterer, if possible, while some of the wave will be reflected back away from the scatterer [29]. When waves are reflected, the time needed for the reflected wave to return to the transducer, or another transducer will be

dependent on the distance through which the wave travels and the speed of sound properties of the material [29]. Therefore defects can be located by measuring the changes in time of flight from some reference point, typically a back wall of the tested piece [29, 31]. For example, figure 2.1 shows how an ultrasound setup could be used to determine the location of a defect.

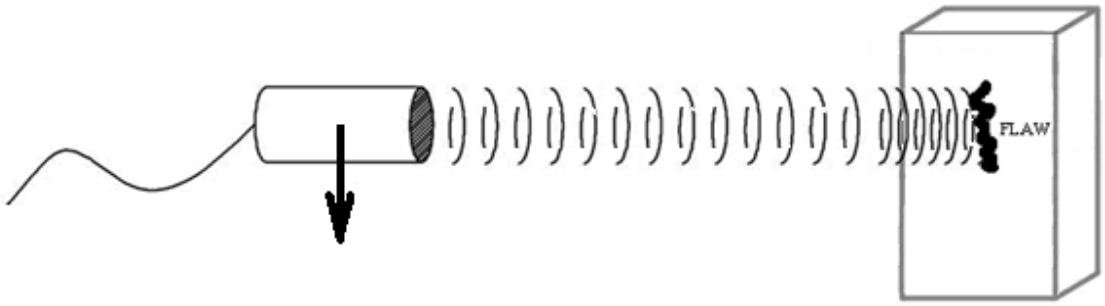

Figure 2.1: Illustration of ultrasonic flaw detection using pulse-echo techniques. Transducer is moved down the length of the object while scanning so that a flaw can be discerned from the back wall.

Figure 2.1 shows a pulse-echo test in which a single transducer aligned normally to the surface is used to both generate and receive the ultrasonic signal. The time of flight changes depending on whether or not the signal encounters a flaw before the back wall. If the speed of sound of the material is known, this method allows for the depth of the flaw to be determined.

Acoustic waves are also affected by attenuation which can be used as a measurement when using non-destructive testing techniques [31]. Attenuation is the nature of the amplitude of a wave to decrease while it propagates through a material [29]. A practical demonstration of this is how the volume of a person's

voice seems to drop as they move away from the listener. The main cause of attenuation is the absorption of the wave's energy by the material [29]. The rate of attenuation is a material property that is dependent on the frequency of the propagated wave [29]. If both the diffraction attenuation and the velocity dispersion are known, then the average size of the scatterer can be determined [32].

2.2.2 Ultrasonic Properties and Applications

Ultrasonic inspection methods have played an important role in the evaluation of the structural infrastructure of society as the bridges, buildings, boats, and as highway systems have grown older and begun requiring maintenance and replacement [27]. Ultrasound is capable of locating steel supports within a building structure, measuring the thickness of a concrete foundation, as well as locating any defects within the interior of the structure [30]. Ultrasound has proven to be very reliable in the testing of welds as it can detect any voids along the weld seam as well as evaluate the surrounding metals strength changes due to the heat treatment [30]. Casting processes also typically rely on ultrasound because it can determine the state of the curing process as well as give a good indication of how the surface finish will turn out before the

cure is even finished [27, 28]. Most importantly, ultrasonic testing is relatively cheap and does not require much training to be able to use [27].

Traditionally, when performing ultrasonic tests, correlations are made between the ultrasonic variables, such as attenuation and speed of sound, and material properties such as hardness, curing condition, and fracture resistance [27]. While these correlations may have a good fit for one species of materials, they may not fit for others because the microstructural differences such as grains and porosities will affect the ultrasonic parameters [27]. While ultrasonic testing has been a commonly used and reliable inspection technique for quite some time, there is not a considerable amount of literature concerning ultrasonic testing of geopolymeric material. For this reason, the few papers concerning ultrasonic testing of geopolymers were supplemented with other papers that use ultrasound to study the curing rates of traditional ceramics because of the similar nature of these types of materials. The Young's modulus and Poisson's ratio of a material can be derived as a function of the speed of sound of a material in both the shear and longitudinal wave modes [29, 31, 33]. Using this technique to investigate the properties of alumina ceramics and concrete, it was discovered that the speed of sound of the material decreased approximately proportionally with an increase in porosity [33, 34]. This had a similar effect on Young's modulus and Poisson's ratio, both decreasing as the porosity of the sample

increased [33]. It is also worthwhile to note that this study determined the longitudinal velocity to be roughly twice that of the shear velocity, a trend which is common for most materials [31, 33]. In a separate study focusing on using geopolymers as a part of a composite material, the speed of sound and attenuation of cement, fly ash based geopolymers, and fly ash cement composites were all documented as a function of time during curing and it was discovered in each case that the speed of sound increased as the structure became more rigid during curing while the attenuation for each would fluctuate initially, and begin to rapidly drop off after the materials begin to set [25].

Chapter 3

Theory

3.1 Relationship Between the Speed of Sound and the Elastic Properties

Ultrasonic waves, like all sound waves, propagate by vibrating molecules within the material that the wave travels through in a sinusoidal fashion. Longitudinal waves cause displacements along the same direction that the wave propagates, while shear waves cause displacements in a direction that is normal to the direction of propagation. As these waves travel, the particles oscillate with respect to both time and position. Therefore, a model of either of these waves must include some dependence on the frequency of both time and space. The angular frequency, ω, is used to show how the wave oscillates with respect to time while the wave number, k, is used as a spatial frequency. The angular frequency and wave number can be defined as:

$$\omega = 2\pi f$$
$$k = \frac{\omega}{c} \tag{3.1}$$

Where f is the frequency of the wave in Hertz and c is the speed of sound in [m/s].

Understanding the nature of a wave propagating through a three dimensional structure is easier if a simpler one dimensional wave is examined first. For the simple case of a one dimensional wave propagating in a direction arbitrarily chosen to be x, the model for the ultrasonic wave can be given as:

$$u(x,t) = u_0 \cos(\omega t - kx) \tag{3.2}$$

Where u_0 is the maximum amplitude of the displacement, u. The displacement can be assumed to be either along x, or normal to it making this model valid for both shear and longitudinal waves. Taking the partial derivative twice of u(x,t) with respect to position will yield:

$$\frac{\partial^2 u}{\partial x^2} = -u_0(-k)^2 \cos(\omega t - kx) \tag{3.3}$$

Likewise, taking the partial derivative twice of u(x,t) with respect to time will yield:

$$\frac{\partial^2 u}{\partial t^2} = -u_0(\omega)^2 \cos(\omega t - kx) \tag{3.4}$$

Equations (3.3) and (3.4) can be rewritten in terms of the original equation, (3.2) so that:

$$\begin{aligned} \frac{\partial^2 u}{\partial t^2} &= -\omega^2 u(x,t) \\ \frac{\partial^2 u}{\partial x^2} &= -k^2 u(x,t) \end{aligned} \tag{3.5}$$

Rewriting (3.5) and setting the equations equal to each other will produce the 1-dimensional wave equation given as:

$$\frac{\partial^2 u}{\partial x^2} - \frac{1}{c^2}\frac{\partial^2 u}{\partial t^2} = 0 \tag{3.6}$$

Now, consider a small differential element undergoing a simple normal stress, σ_{xx} as shown in figure 3.1a.

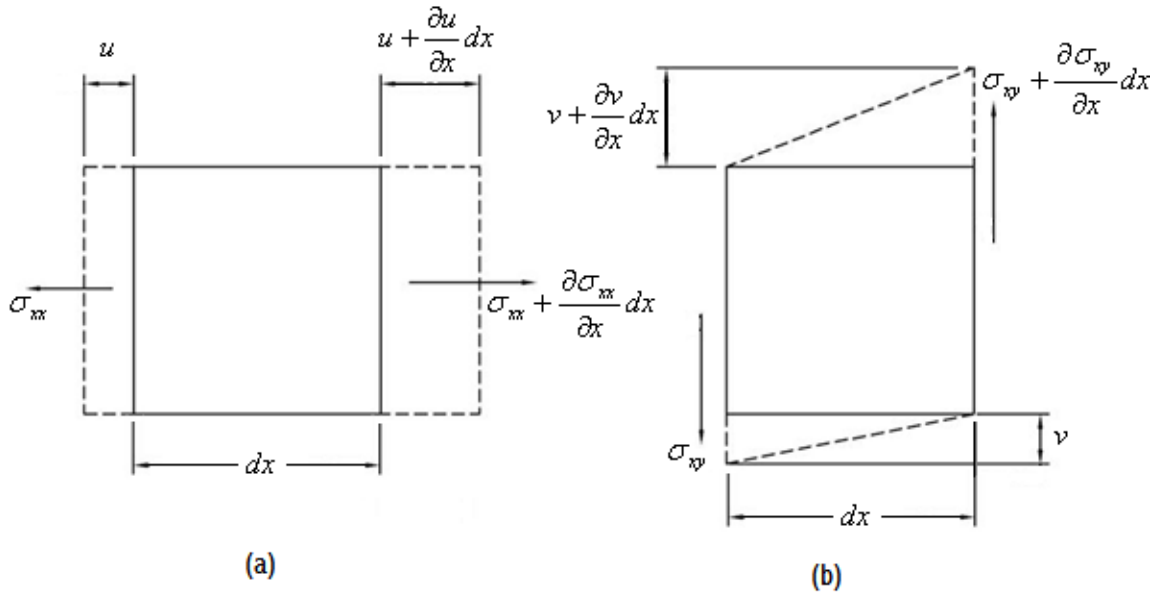

Figure 3.1: Differential stress elements for (a) simple longitudinal stress and (b) simple shear stress.

From Newton's First Law a force balance can be applied to this differential element assuming a uniform cross sectional area, A, so that:

$$\left[\left(\sigma_x+\frac{\partial \sigma_x}{\partial x}dx\right)-\sigma_x\right]A=\frac{d}{dt}\left[m\frac{\partial u}{\partial t}\right] \tag{3.7}$$

Assuming that the mass, m, remains constant, the mass can be written in terms of the density, ρ, and moved outside the derivative.

$$\frac{\partial \sigma_x}{\partial x}dxA=\rho dxA\frac{\partial^2 u}{\partial t^2} \tag{3.8}$$

Finally, the above equation can be simplified to:

$$\frac{\partial \sigma_x}{\partial x}=\rho\frac{\partial^2 u}{\partial t^2} \tag{3.9}$$

Because the material is deforming elastically in one dimension, the longitudinal stress and strain can be related by the elastic modulus for isotropic materials.

$$\sigma_x = E\varepsilon = E\frac{\partial u}{\partial x} \tag{3.10}$$

Where E is the elastic modulus and ε is the strain. Taking the partial derivative of the above equation with respect to x will yield:

$$\frac{\partial \sigma_x}{\partial x} = E\frac{\partial^2 u}{\partial x^2} \tag{3.11}$$

Equations (3.9) and (3.11) can be easily combined and rewritten in a form that is correspondent to the one dimensional wave equation.

$$\frac{\partial^2 u}{\partial x^2} - \frac{1}{c^2}\frac{\partial^2 u}{\partial t^2} = 0 \tag{3.12}$$

Therefore, comparing equations (3.11) and (3.12), the speed of sound for the longitudinal case can be written in terms of the elastic properties of the material as:

$$c_l = \sqrt{\frac{E}{\rho}} \tag{3.13}$$

Where c_l is the longitudinal speed of sound. This same approach can be applied to shear waves, such as those shown in Figure 3.1b. In the case of the shear wave, the stress and strain are related by the shear modulus, G, so that the eventual speed of sound can be written as:

$$c_s = \sqrt{\frac{G}{\rho}} = \sqrt{\frac{E}{2\rho(1+\upsilon)}} \tag{3.14}$$

Where υ in the above equation refers to the Poisson's ratio which is unitless.

When a three-dimensional differential element is examined in a similar manner, deflections due to Poisson's effects will also occur. Therefore, if a longitudinal stress is applied along the x axis, there will be a deflection, u, along x as well as deflections, v and w, along y and z respectfully. Considering these additional deflections and the assumed isotropic nature of the material, the stress and strain for a three dimensional body can be related by:

$$\varepsilon_{ii} = \frac{1}{E}\sigma_{ii} - \frac{\upsilon}{E}\left(\sigma_{jj} + \sigma_{kk}\right) \tag{3.15}$$

$$\varepsilon_{ij} = \varepsilon_{ji} = \frac{1}{2G}\sigma_{ij} \tag{3.16}$$

Where the dummy variables i, j, and k are used to represent the x, y, and z directions. Equations (3.15) and (3.16) can be expanded to create a total of 6 equations in which the 6 different strains are given as a function of the 6 different stresses. For the purposes of this analysis, it is simpler to work with the stress as a function of strain, so the above equations can be rewritten so that:

$$\sigma_{ii} = \frac{E(1-\upsilon)}{(1+\upsilon)(1-2\upsilon)}\varepsilon_{ii} + \frac{\upsilon E}{(1+\upsilon)(1-2\upsilon)}\left(\varepsilon_{jj} + \varepsilon_{kk}\right) \tag{3.17}$$

and,

$$\sigma_{ij} = \frac{E}{(1+\upsilon)}\varepsilon_{ij} = \frac{E}{(1+\upsilon)}\varepsilon_{ji} \tag{3.18}$$

At this point, carrying the above coefficients can become difficult and complicated, making the mathematics prone to errors. As a means of simplifying

the notation, the Lamé coefficients, shown below, are introduced at this point so that the stress-strain relationships can be simplified.

$$\lambda = \frac{\upsilon E}{(1+\upsilon)(1-2\upsilon)} \tag{3.19}$$

$$\mu = \frac{E}{2(1+\upsilon)} \tag{3.20}$$

With the use of the Lamé coefficients, the stresses and strains can be more simply related to each other as:

$$\begin{pmatrix} \sigma_{xx} \\ \sigma_{yy} \\ \sigma_{zz} \\ \sigma_{yz} \\ \sigma_{xz} \\ \sigma_{xy} \end{pmatrix} = \begin{bmatrix} (2\mu+\lambda) & \lambda & \lambda & 0 & 0 & 0 \\ \lambda & (2\mu+\lambda) & \lambda & 0 & 0 & 0 \\ \lambda & \lambda & (2\mu+\lambda) & 0 & 0 & 0 \\ 0 & 0 & 0 & 2\mu & 0 & 0 \\ 0 & 0 & 0 & 0 & 2\mu & 0 \\ 0 & 0 & 0 & 0 & 0 & 2\mu \end{bmatrix} \begin{pmatrix} \varepsilon_{xx} \\ \varepsilon_{yy} \\ \varepsilon_{zz} \\ \varepsilon_{yz} \\ \varepsilon_{xz} \\ \varepsilon_{xy} \end{pmatrix} \tag{3.21}$$

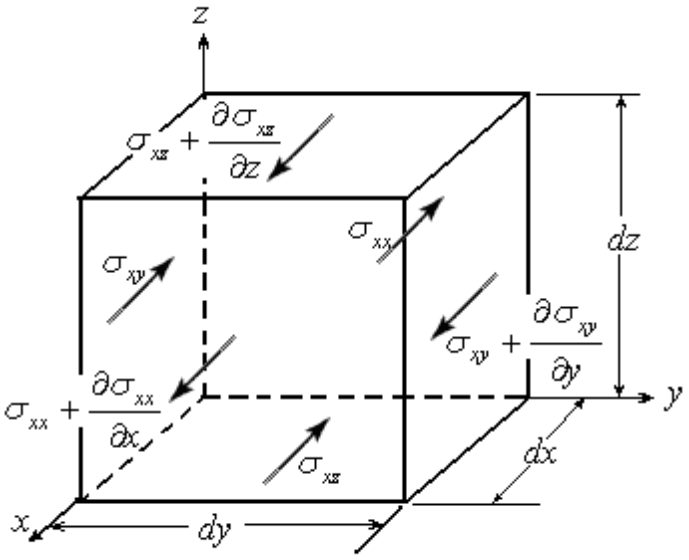

Figure 3.2: Stresses along the x-direction acting upon a 3-dimensional differential element.

Now, figure 3.2 depicts a differential element undergoing stresses in the x-direction due to an ultrasonic wave. Applying Newton's second law, the force balance will produce:

$$\begin{aligned}\frac{\partial^2 u}{\partial t^2}\rho dxdydz = &\left(\sigma_{xx}+\frac{\partial\sigma_{xx}}{\partial x}dx\right)dydz-\sigma_{xx}dydz+\left(\sigma_{xy}+\frac{\partial\sigma_{xy}}{\partial y}dy\right)dxdz\\ &-\sigma_{xy}dxdy+\left(\sigma_{xz}+\frac{\partial\sigma_{xz}}{\partial z}dz\right)dxdy-\sigma_{xz}dxdz\end{aligned} \tag{3.22}$$

This same procedure can be applied to deflections in the other two directions as well. After simplification, this will result in:

$$\begin{aligned}\rho\frac{\partial^2 u}{\partial t^2} &= \frac{\partial\sigma_{xx}}{\partial x}+\frac{\partial\sigma_{xy}}{\partial y}+\frac{\partial\sigma_{xz}}{\partial z}\\ \rho\frac{\partial^2 v}{\partial t^2} &= \frac{\partial\sigma_{xy}}{\partial x}+\frac{\partial\sigma_{yy}}{\partial y}+\frac{\partial\sigma_{yz}}{\partial z}\\ \rho\frac{\partial^2 w}{\partial t^2} &= \frac{\partial\sigma_{xz}}{\partial x}+\frac{\partial\sigma_{yz}}{\partial y}+\frac{\partial\sigma_{zz}}{\partial z}\end{aligned} \tag{3.23}$$

Rewriting the stress terms from the above equation in terms of the internal strains can be accomplished by substituting the appropriate equations from (3.23) into (3.21). After rewriting to combine similar terms, the 3-Dimensional wave equations can be developed as [36]:

$$\rho\frac{\partial^2 u}{\partial t^2} = (\mu+\lambda)\left[\frac{\partial}{\partial x}\left(\frac{\partial u}{\partial x}+\frac{\partial v}{\partial y}+\frac{\partial w}{\partial z}\right)\right]+\mu\left[\frac{\partial^2 u}{\partial x^2}+\frac{\partial^2 u}{\partial y^2}+\frac{\partial^2 u}{\partial z^2}\right] \tag{3.24}$$

$$\rho\frac{\partial^2 v}{\partial t^2} = (\mu+\lambda)\left[\frac{\partial}{\partial y}\left(\frac{\partial u}{\partial x}+\frac{\partial v}{\partial y}+\frac{\partial w}{\partial z}\right)\right]+\mu\left[\frac{\partial^2 v}{\partial x^2}+\frac{\partial^2 v}{\partial y^2}+\frac{\partial^2 v}{\partial z^2}\right] \tag{3.25}$$

$$\rho \frac{\partial^2 w}{\partial t^2} = (\mu + \lambda)\left[\frac{\partial}{\partial w}\left(\frac{\partial u}{\partial x} + \frac{\partial v}{\partial y} + \frac{\partial w}{\partial z}\right)\right] + \mu\left[\frac{\partial^2 w}{\partial x^2} + \frac{\partial^2 w}{\partial y^2} + \frac{\partial^2 w}{\partial z^2}\right] \tag{3.26}$$

At this point, it is necessary to reflect on the nature of the wave which is being investigated. Both longitudinal and shear waves will have oscillations as they propagate through the material. Therefore each wave's oscillations should be a function of both time and position with the main difference between the two types of waves being the direction of the oscillation. If the wave is propagating in the longitudinal mode so that all of its energy is traveling in the x-direction, then any of the cross derivatives will go to zero leaving only the $\frac{\partial^2 u}{\partial x^2}$ terms.

Therefore, Equation 3.24 shows that the wave velocity traveling in this fashion will have a speed of sound

$$c_l = \sqrt{\frac{2\mu + \lambda}{\rho}} = \sqrt{\frac{E(1-\upsilon)}{\rho(1+\upsilon)(1-2\upsilon)}} \tag{3.27}$$

Similarly, equations (3.25) and (3.26) both show that a shear wave traveling along the x-direction will have a wave velocity,

$$c_s = \sqrt{\frac{\mu}{\rho}} = \sqrt{\frac{G}{\rho}}\sqrt{\frac{E}{2\rho(1+\upsilon)}} \tag{3.28}$$

Now that the speeds of sound have been determined as functions of the elastic properties, learning how the elastic properties depend upon the speed of sound is a simple matter of algebra. Solving for Young's modulus and the Poisson's ratio will finally yield:

$$E = \rho C_S^2 \left(\frac{3C_l^2 - 4C_S^2}{C_l^2 - C_S^2} \right) \tag{3.29}$$

$$\upsilon = \frac{1 - 2\left(\frac{C_S}{C_l}\right)^2}{2 - 2\left(\frac{C_S}{C_l}\right)^2} \tag{3.30}$$

3.2 Determination of Time of Flight.

The speed of sound through a material is determined empirically by measuring the time of flight of a sound wave. When analyzing sound waves, the time of flight is the time elapsed between each pulse along the A-line viewed with an oscilloscope which is equivalent to the time necessary for the energy of the wave to traverse the given distance. A-lines plot the amplitude of the voltage of the signal as a function of time, and example of an A-line from a pulse-echo scan from a longitudinal transducer is shown in figure 3.3.

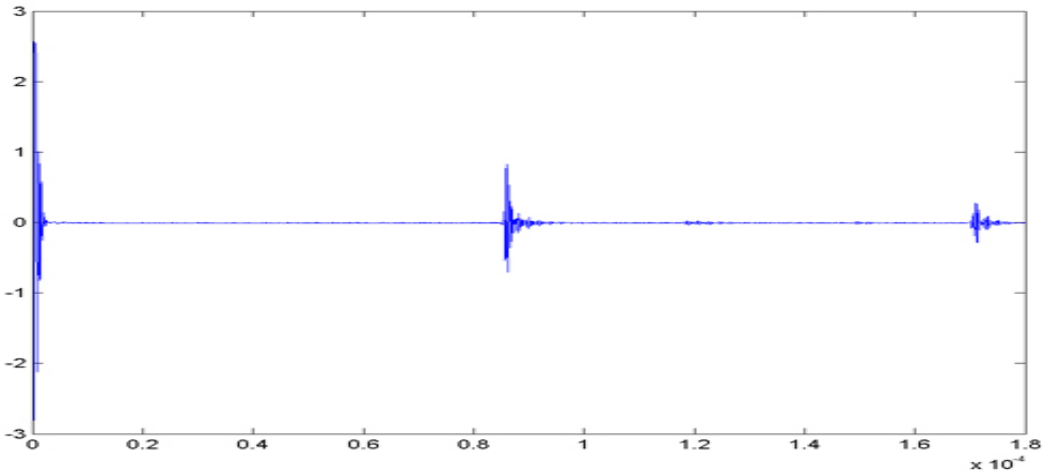

Figure 3.3: Example A-line.

There is an "initial bang" that occurs at the triggering of each signal causing a displacement to occur near the origin of the time scan. The initial bang is a high amplitude oscillation perceived by the equipment as the instrumentation triggers and can be seen at the far left of the A-line plot in figure 3.3. This effect is expected and is not considered when evaluating the signal. Furthermore, two signals are visible in this A-line. If it is assumed that the transducer is placed directly in contact with the specimen being scanned, then the first signal is caused by the initial reflection from the back wall of the sample. However, some of the signal does not return directly to the transducer and is reflected again off of the front wall so that it traverses the thickness of the sample twice causing a signal to appear at a distance twice the first one. These reflected signals will continue to appear until the signal disappears due to attenuation of the energy of the wave.

The speed of sound is simply calculated as the distance traveled by the sound wave, being twice the thickness of the specimen for the case of pulse-echo transmission with the transducer in contact with the specimen, divided by the amount of time needed for the sound wave to traverse that distance. Determining the thickness of the sample material is a simple process that can be measured through any number of techniques and the time needed for the signal to travel through the material is determined from the A-line. However, depending on how the test is set up, different calculations for the speed of sound must be used.

Pulse-echo scans are the simplest when it comes to evaluating the speed of sound. The time of flight is actually the time needed for the sound wave to travel the thickness of the sample, bounce off of the back wall, and then return to the transducer. Therefore the speed of sound is actually twice the distance, d, divided by the time of flight,t.

$$C = \frac{2d}{t} \tag{33}$$

However, if a couplant is used to transmit the signal from the transducer to the sample, there may be complications due to the echo off of the front surface of the sample and the time needed for the sound wave to traverse through the couplant. This study uses only contact pulse-echo methods with thin film couplants so any effects caused by this are considered negligible.

Transmit-receive scans behave much like pulse-echo scans except that a second transducer is used to receive the signal so that the speed of sound is equivalent to the time of flight divided by the thickness of the material. However, due to the testing set up in this study, the couplant effects are not negligible and must be considered. Water was the couplant chosen due to its availability, negligible attenuation over the distances used in this study, and the fact that its speed of sound has been well documented as a function of temperature [37]. In order to determine the speed of sound of a sample material, two tests must be considered, one where the sample is in the path of the sound wave and one where no sample is present so that the sound wave traverses only through water. Figure 3.4 depicts these two cases while providing a nomenclature for the lengths associated in the analysis.

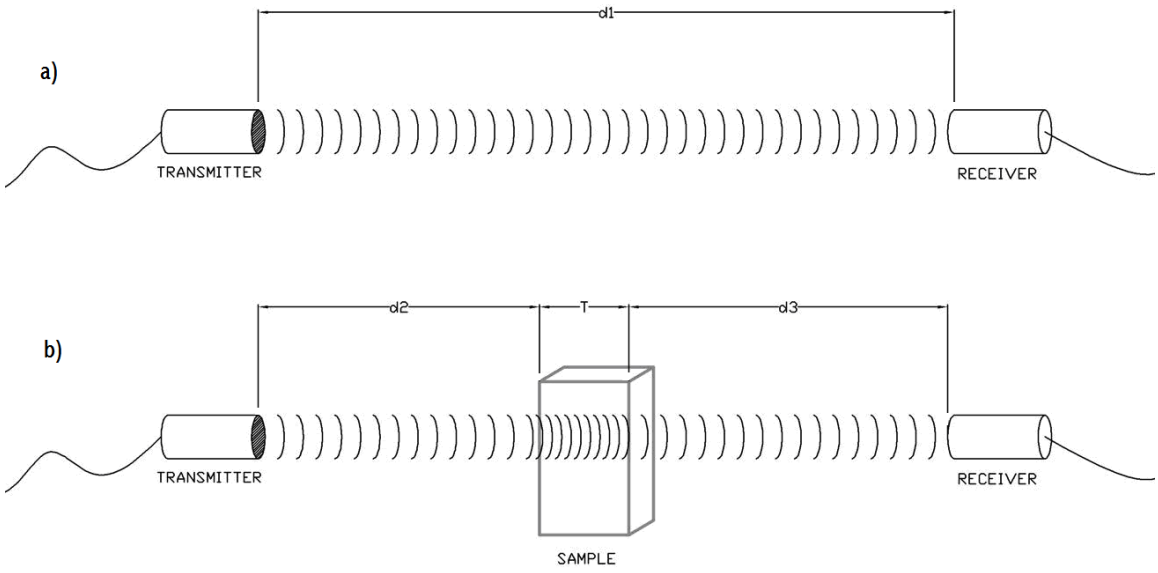

Figure 3.4: Transmitter alignment for longitudinal wave scanning procedure.

In the above figure d_1, d_2, and d_3 are distances through which the sound wave travels through water and T is the thickness of the material being scanned. Since the speed of sound through water is known, the time of flight for the case of Figure 4.4a can be written as

$$t_1 = \frac{d_1}{c_W} \tag{34}$$

where t_1 is the time measured for a sound wave to traverse the distance d_1 and c_w is the speed of sound through water. The time of flight for the case of Figure 3.4b can be similarly written as the summation of the time of flight of each distance such that:

$$t = \frac{d_2}{c_W} + \frac{d_3}{c_W} + \frac{T}{c_{l,Sample}} \tag{35}$$

Where $c_{l,sample}$ is the speed of sound through the sample and t is the recorded time of flight. The speed of sound through the sample is the value of importance in this equation, so solving for $c_{l,sample}$ provides the equation:

$$c_{l,Sample} = \frac{T}{t - \left(\frac{d_2 + d_3}{c_W} \right)} \tag{36}$$

The distances, d_2 and d_3 could be measured and substituted directly into equation (3.36) to solve for the speed of sound, however making such a measurement is difficult and would need to be reevaluated every time a sample is switched. Instead, d_2 and d_3 will be substituted with other known values

obtained from the orientation of the setup. Because the transducers are kept at the same position with respect to each other, the distances can be equated to each other so that,

$$d_1 = d_2 + d_3 + T \tag{37}$$

The distance d_1 was already determined in terms of the time of flight without a sample and the speed of sound through water so that the above expression can be rewritten as

$$d_2 + d_3 = t_1 c_W + T \tag{38}$$

Substituting this back into the speed of sound through the sample will provide:

$$C_S = \frac{T}{t_{measured} - t_1 + \frac{T}{C_W}} \tag{39}$$

This final equation is written in terms of values that can easily be measured so that quick calculations can be made for a sample scanned in this fashion.

3.3 Time-Frequency Analysis

3.3.1 Need for Time-Frequency Analysis.

Waves traveling through a viscoelastic media are subject to damping due to both attenuation and dispersion [36]. Attenuation, in ultrasonic imaging, is

due to two factors: absorption and scattering [29]. The absorption contribution is due to the natural damping nature of the material during vibrations while the scattering contribution is due to the reflection of the signal away from the receiving transducer whenever a discontinuity in phase is encountered such as a pore, crack, material surface, or patch of unreacted material within a geopolymer.

Dispersion is the effect of damping of specific frequencies of a wave when a wavepacket consisting of more than one frequency travels through a viscoelastic medium. If a wave of a single phase were to travel through a medium, then its speed of sound would be written as a function of the frequency and wave number similar to equation 3.1, but now with a subscript phi to differentiate that this is a specific phase speed.

$$c_{\phi} = \frac{\omega}{k} \tag{3.40}$$

Now, if a wave consisting of several different phases or frequencies, such as that of a typical ultrasonic signal, superimposed on one another were to travel through the same medium then the speed of each phase would need to be a function of the wave number. Otherwise, the two different phases would separate from each other. In reality, the energy of a wave consisting of several frequencies travels as a constant group speed and the energy of any specific phase cannot exceed this speed. Therefore waves with a longer wavelength, or a

smaller wavenumber, will travel faster than those with a shorter wavelength and the wavepacket. This will cause the wavepacket to alter with time as specific frequencies become damped as they reach the front of the wavepacket.

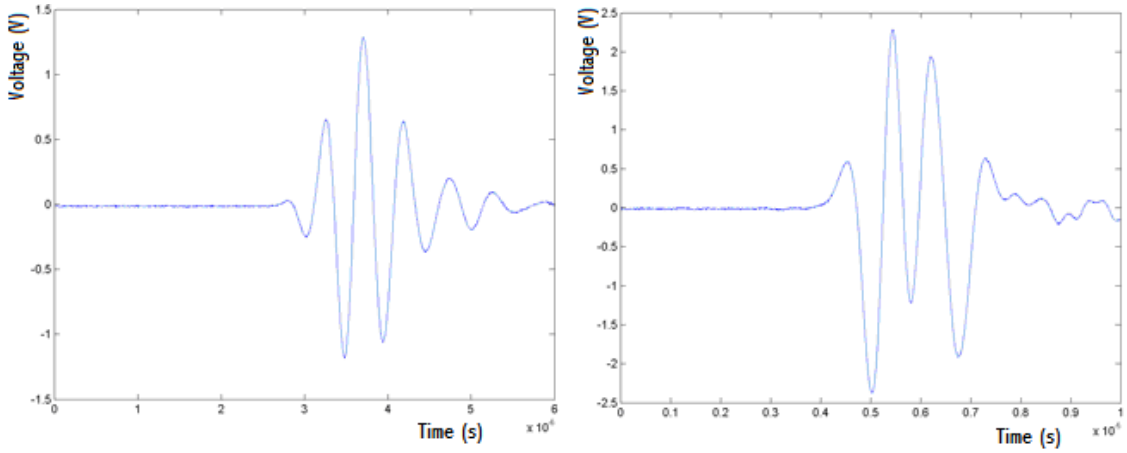

Figure 3.5: A signal transmitted directly through water showing negligible signs of dispersion and attenuation (left) and a signal transmitted through a geopolymer sample showing both dispersion and attenuation effects (right).

Practically, dispersion and attenuation can make ultrasonic imaging very difficult. Figure 3.5 shows how a signal transmitted through a viscoelastic medium can experience dispersion and attenuation. The figure on the left is an ideal image of an A-line. However, the figure on the right has had some of its peaks altered in both amplitude and position. Furthermore, there is also the presence of obvious noise following the signal which may be superimposed into the main signal as well. Since determining the speed of sound is dependent on determining the time of flight, it may become difficult to use a signal such as the one on the right to determine at what point this signal has arrived. Therefore, a

technique that would determine the phase velocity would be useful in evaluating the actual group speed of sound

3.3.2 Wigner Transform and Determination of Phase Velocity.

There are several methods available to determine the frequency content of a signal. The most basic method of evaluating the frequency content of the signal is with the use of the Fourier transform. With this method, a signal generated in the time domain can be transformed to determine the overall frequency of the signal. The downside to this technique is that it only determines which frequencies are present; it provides no knowledge of when the frequency occurred or for what duration [38]. One method to overcome this problem is with the use of the short-time Fourier transform (STFT) which is arguably the most widely used time-frequency technique [38]. The STFT utilizes a windowing function to determine when the frequencies occur in time. This means that a small section, or window, of a signal will be analyzed using the Fourier transform. This window will then be moved to the next section of the signal where the Fourier transform will again be performed. This process is continued until the windowing function has been moved across the entire signal. This is a powerful and relatively simple technique that is also well known [38]. However

there are limitations to this method as well. According to the Heisenberg uncertainty principle, STFT cannot provide good resolution in both time and frequency [38]. If the windowing function becomes too small, providing good resolution in time, then the signal itself becomes distorted and the frequency spectrum will become unrelated to the actual signal [38]. Likewise, if the signal becomes broad, there will be much better resolution of the frequencies but the time resolution will suffer [38].

This study chose to use the Wigner-Ville distribution to study the time-frequency relationship of the ultrasonic signal. The actual Wigner-Ville transform can be obtained from the equation:

$$\begin{aligned} W(t,\omega) &= \frac{1}{2\pi}\int_{-\infty}^{+\infty} s*\left(t-\frac{1}{2}\tau\right)s\left(t+\frac{1}{2}\tau\right)e^{-i\tau\omega}d\tau \\ &= \frac{1}{2\pi}\int_{-\infty}^{+\infty} S*\left(\omega-\frac{1}{2}\theta\right)S\left(\omega+\frac{1}{2}\theta\right)e^{-it\theta}d\theta \end{aligned} \tag{3.41}$$

Where τ is a differential step in the time domain and θ is a differential step in the frequency domain. This specific density function will provide the energy density of the signal as a function of both time and frequency. The time of flight for a specific frequency will then be determined as the time with the maximum amplitude for the specific frequency.

The Wigner-Ville transform is a good choice for this study because it will provide a continuous distribution with respect to both time and frequency and

does not require any windowing function. However, there is a major disadvantage to this technique in that it can introduce artifact signals at locations where no signal is present [38]. From equation 3.41 it can be seen that the Wigner-Ville transform calls upon a value of the signal at a differential step before and after a given time. Should a signal have a zero amplitude for a given time and intensity, the Wigner-Ville transform may incorrectly create a signal, or artifact, there due to the amplitude of the signal surrounding that specific time and frequency. However, if the signal occurs entirely within some specific time or frequency range, there cannot be any artifact signals outside of this range. This is because of the same principle that creates the artifacts; if the signal is zero for every time step before or after a given time value then the Wigner-Ville transform will always be zero outside of that range. A certain amount of a priori knowledge of the signal must be known to reduce this problem for the purpose of this study. Viewing this signal in the time domain, it is fairly obvious which part of the signal contains the information of interest. If the portion of the signal containing the energy is analyzed separately from the rest, then the noise occurring outside the area of interest will not be able to introduce any artifacts. This is not a windowing function in the sense of the STFT but a truncation of the signal outside of a determined time range.

The final concern that arises from the use of the Wigner-Ville distribution comes from the use of numerical techniques to evaluate the integral. The use of time steps of ±½τ implies that there must be discrete values between the samples values. Since the signals used in this study are composed of discrete data points and not a continuous function, the signal must be interpolated to over sample by a factor of two.

3.3.3 Group Velocity.

The Wigner-Ville distribution will determine the phase velocity, however it has already been stated that the velocity of each particular phase will differ from the actual group speed of sound. The group velocity for a wave packet containing a continuous frequency spectrum can be obtained by [36]:

$$c_g = \frac{d\omega}{dk} \tag{3.42}$$

This equation can then be rewritten as [36]:

$$c_g = \frac{c_\phi}{1 - \frac{\omega}{c_\phi}\frac{\partial c_\phi}{\partial \omega}} \tag{4.43}$$

Since the values actually used in this study are located at discrete frequencies, the partial derivative must be computed using a finite difference technique. The

average value of the group velocity for each phase velocity step is then computed to be used as the speed of sound.

Chapter 4

Experimental Setup

4.1 Synthesis of Geopolymer Samples

4.1.1 Sample Compositions

Geopolymer samples were created to obtain a range of silicon to aluminum ratios ranging from around 1.5 to 6.4. The curing regiments, material sources and activating solutions were kept constant for all tests in order to eliminate as many variables as possible and focus the study onto the changing characteristics of the elastic properties due to the Si:Al ratio. The components used to produce activating solution consisted of sodium hydroxide (NaOH) purchased from Fischer Scientific, E™ sodium silicate produced by PQ Corporation with a 3.22 weight ratio of SiO_2:Na_2O, and tap water. MetaMax, a commercially available calcined kaolin clay produced by the Englehard Corporation, and reagent grade amorphous silica produced by Fischer Scientific were chosen for the source materials. Metamax, whose composition is provided in table 4.1, was chosen as the main source of the needed 4-coordinated alumina for the reactions due to the fact that it introduces less additional chemicals compared to other metakaolin products available on the market.

Table 4.1: Chemical composition of MetaMax (*Material Lost on Ignition) [39]

Compound	SiO_2	Al_2O_3	Na_2O	K_2O	TiO_2	Fe_2O_3	CaO	MgO	P_2O_5	SO_3	LOI*
Percent Composition	53.0	43.8	0.23	0.19	1.70	0.43	0.02	0.03	0.03	0.03	0.46

The process for preparing geopolymers is relatively simple and followed the following process:

1) Sodium hydroxide (NaOH) is added to water so as to create a 15 molal NaOH solution. The dissolution of NaOH into water is an exothermic reaction; therefore, the solution should be mechanically stirred until the solution returned to room temperature.
2) An amount of sodium silicate needs to be measured so as to be double the mass of the NaOH solution. This sodium silicate is then added to the NaOH solution and mechanically mixed until the new mixture also returned to room temperature. If allowed to set open to the atmosphere, the activating solution will begin to solidify and become unusable for geopolymerization, therefore it is important to use this solution immediately after mixing.
3) Metakaolin and amorphous silica should then be measured out so as to obtain the intended Si:Al ratio while also maintaining approximately 33% water by weight, where the water composition includes the water used to dissolve the sodium hydroxide as well as the water within the sodium silicate.
4) The metakaolin and silica are then slowly added to the mixture so that a mechanical mixer can effectively stir the solution without jamming.

5) After all of the activating ingredients were thoroughly mixed, the slurry is poured into 50mm plastic cube molds. These molds are vibrated for ten minutes to remove the presence of air pockets trapped during the casting process and should then be sealed with plastic wrap to entrap water which is necessary for the geopolymerization reaction.
6) Each sample is allowed to cure in an oven at 65°C for 24 hours before being removed from the mold.

4.1.2 Sample Water Content Concerns

Initial attempts to cast geopolymers for this study used only metakaolin and activating solution; no amorphous silica was added independently. In order to maintain similar activating solution for each sample, the kaolin was the only adjustable source of aluminum in the samples. Therefore, the Si:Al ratio was lowered by adding more metakaolin and increased by using less metakaolin. Many of these geopolymer samples had difficulty hardening after only 24 hours of curing, and some failed to fully harden even after curing for 4 days at temperatures exceeding 100°C. From a qualitative examination, the effectiveness of the geopolymerization was based on the theoretical Si:Al ratio of the samples. Lower Si:Al ratios at or below 1.7 behaved as expected being fully set after only 24 hours without any cracking, however as the Si:Al ratio increased the samples

would cure with cracks, or break when submerged into water if they were even capable of curing at all. It was assumed that the cause of these defects in higher Si:Al samples was a result of a higher percentage of water in the composition which caused cracks when escaping from the material due to evaporation or prevented the material from completely hardening giving it a consistency similar to putty rather than a ceramic. In order to alleviate this problem, amorphous silica was added to increase the theoretical Si:Al ratio without needing to use an excessive weight percentage of water. A mass ratio approximately 33% water was deemed to be acceptable based on the observed trend, and a complete set of new compositions was created so as to avoid this problem. This theory later proved itself to be valid when, after three months, an original sample shown in figure 4.1 finally hardened with a significant decrease in volume due to the evaporation of the water. The sample shown in figure 4.1 was originally casted so that the material was flush with the surface of the mold. The fact that the end product contains cracks from escaping water and the sides have receded away from the sides of the mold signifies that a significant amount of mass was lost to evaporation.

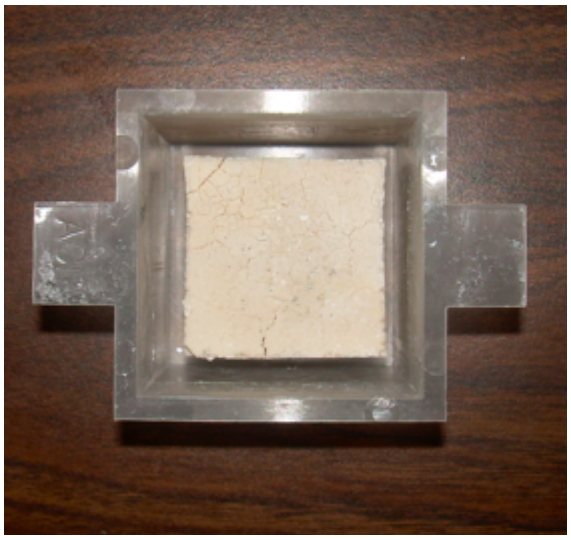

Figure 4.1: Failed geopolymer samples with Si:Al ratios of 4.743 after completely curing

Seven different samples were successfully made for this study. The Si:Al ratios range from 1.49 to 6.4 as described in table 4.2. Each sample set consisted of at least three casted 50mm cubes. For the purpose of convention, the samples are referred to by their respective Si:Al ratios. Other ratios have also been used in literature to describe the nature of geopolymers. Typically, the ratios include the chemicals that constitute the geopolymerization such as silica (SiO_2), alumina (Al_2O_3), water, and the alkali activator (M_2O). However, the contributions of the water and alkali activator come exclusively from the activating solution which was kept constant to reduce the variables. Therefore, any relationship based on these chemical ratios will be trivial due to there minute variances. Instead, the only chemical ratio considered for this study is the Si:Al ratio. The SiO_2:Al_2O_3 ratio is also commonly used to compare characteristics but doing so in addition

to the Si:Al ratio would be redundant in this instance. However, the molar ratios for the final samples in terms of both Si:Al and SiO_2:Al_2O_3 are available in table 4.2 as a comparison reference.

Table 4.2: Chemical ratios of the prepared samples.

Ratio	Sample #1	Sample #2	Sample #3	Sample #4	Sample #5	Sample #6	Sample #7
Si:Al	1.49	1.52	1.9	2.2	3.1	4.1	6.4
SiO_2:Al_2O_3	2.99	3.04	3.7	4.9	6.2	8.2	12.8

4.1.3 Sample Finishing Processes

The equations derived for the speed of sound in the previous chapter are dependent on the material being isotropic. While no study has ever considered this type of material to behave anisotropically, there was concern that the open surface on only one side may cause the material to behave differently along different directions. To test whether this was occurring or not, each sample was tested along three orthogonal directions. It is assumed that if the properties remained consistent in each direction, that the material could be considered isotropic. As a means of distinguishing between different directions within the material, each sample was marked along its edges to signify three different directions referred to by x, y and z. The x and y directions were arbitrarily chosen to go along the sides of the samples as they were cast, while the z

direction was always chosen as the direction extending from the bottom surface to the top surface, as the blocks were cast.

The first ultrasonic measurements taken of the geopolymer samples were for longitudinal waves using the transmit-receive method in a water tank. This test was conducted using the geopolymer samples in the initial block shape as they were cast before any finishing techniques were completed. Therefore, the edge length of each sample was approximately 50mm. The longitudinal wave method was effective using samples of this size, but when shear waves were used in pulse-echo mode, no return signal was identifiable due to the attenuation of the signal. Therefore each sample was split into three sections, as shown in figure 4.2, so that each sample could still be analyzed with respect to the same scanning directions as was done with the longitudinal mode. The initial cutting was done using a miter saw with a masonry cut off wheel, which was followed by a smoothing with a surface grinder to remove unevenness from the cut and insure that the surfaces remained parallel.

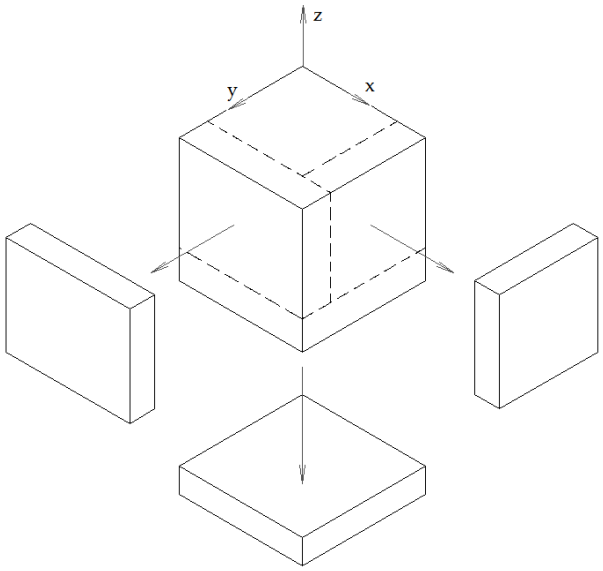

Figure 4.2: Cuts from longitudinal sample to obtain x, y, and z directional shear samples

As mentioned previously, parallelism is important in ultrasonic testing. Should the front and rear surfaces not be parallel, the signal will be deviated away from the transducer in the case of through transmission testing or reflected away from the transducer in the case of pulse echo testing. The current standards for this type of procedure require that the parallelism between the opposing surfaces not exceed 3 degrees [31]. A CMM machine was used to analyze each sample after finishing to determine that it was within this tolerance and also to determine the thickness of the sample.

4.2 Ultrasound Testing

4.2.1 Water Tank Imaging Apparatus

In order to accurately evaluate the longitudinal speed of sound of the samples, a test platform was designed and created to meet the needs of the project as well as the needs for several other future and ongoing projects. These projects required that the test platform be capable of:

1) lateral alignment and adjustability to within a tolerance of 0.5mm
2) have the ability to adjust transducer angles independently to within 0.5°
3) Accommodating a variety of transducer sizes and types
4) performing A-scans, B- scans, C-scans, and Rayleigh scans
5) operating in both pulse-echo and transmit-receive modes

After several design iterations, the final product, shown in figure 4.3, was capable of exceeding all of these requirements. A linear stage motor was used which was capable of lateral translations of 0.02mm while the angular measurements are accurate to half of a minute of arc. A frame structure, shown in figure 4.3, was created to hold the submerged sample and transducers during any scan and remove most degrees of freedom. The one degree of freedom not accounted for by the frame is due to the linear alignment of the transducers

which is compensated for by using linear stage motors. When this setup is run in transmit-receive mode for this study, the transducers are aligned with the motors but then remain stationary during any A-scans or B-scans and the different A-lines are collected by adjusting the sample itself. This adjustment is also performed using similar linear stage motors.

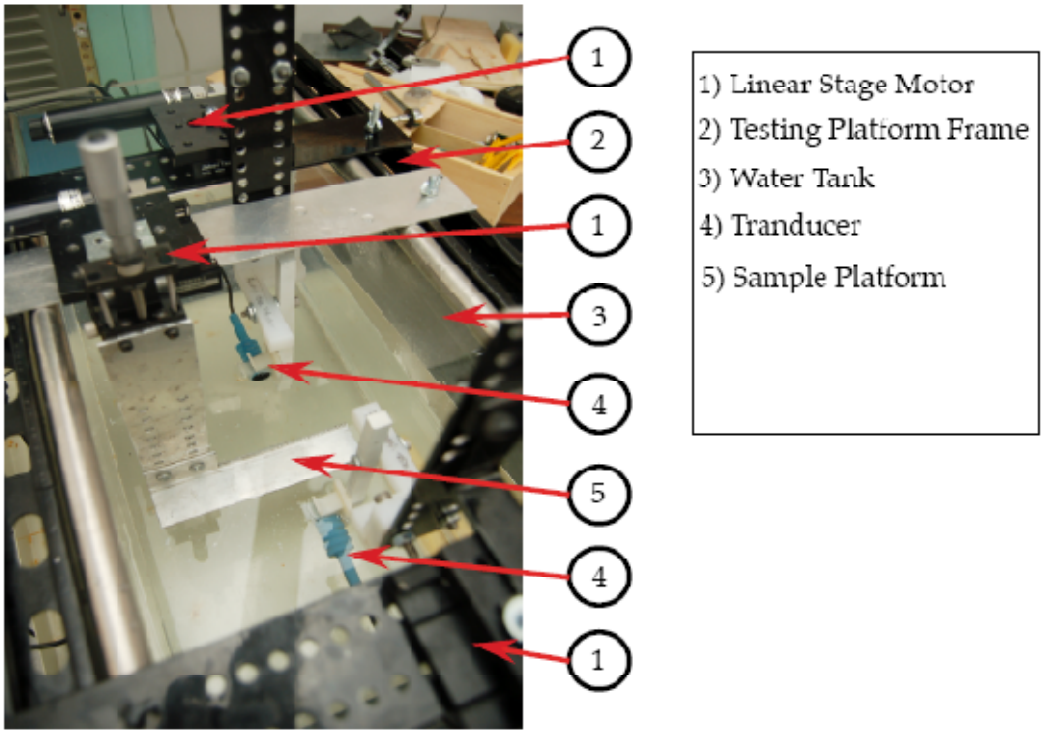

Figure 4.3: Picture of ultrasonic testing platform.

The process of taking longitudinal scans was simplified by the use of a preexisting program written to control the motors from a previous study. This program was designed to perform C-scans with user defined scanning dimensions. Inputing a step size and a number of steps in an x and y direction

defined scanning locations and would cause the motors to move to each scanning location and capture an A-scan which would be saved for future analysis.

Several additional pieces of equipment were also needed in order to generate and view signals produced by the transducers. An oscilloscope, pulser/receiver, and amplifier were also used for the processing of the ultrasonic signals as shown in figure 4.4. The transducers were directly connected to the pulser/receiver which would generate a short pulse and then receive any return signals from the scan. This pulser/receiver was capable of operating in both pulse/echo mode with only one transducer and in through transmission mode with two transducers. The pulser/receiver was also capable of applying a gain to the signal of ±9.9dB. However, if additional gain is necessary, the signal could also be run through the amplifier. The signal from the pulser/receiver or the amplified signal from the amplifier would then be inputted into the oscilloscope where the signals could be recorded.

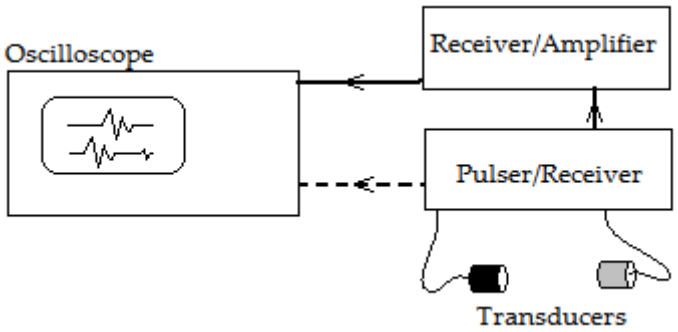

Figure 4.4: Ultrasonic equipment set-up.

4.2.2 Testing Alignment and Setup

Longitudinal speed of sound measurements were taken with the use of the water tank imaging testing platform described in the previous section. Alignment in most degrees of freedom was taken care of by the testing platform itself, however the two transducers still needed to be aligned to insure that they were horizontally in line with one another. To do this, an aluminum test piece was ground flat and placed on the middle platform of the test stand. Each transducer mount had some slop allowed from the bolts that fastened them to the stand which could cause some angular differences. Therefore, each transducer was pointed at the flat test piece and set to scan in a pulse echo mode. The transducer mount was then manipulated until the amplitude of the signal in pulse echo mode reached a maximum value signifying that the transducer face was parallel with the test piece face so as to reflect a maximum amount of energy. After this was done for both transducers, the aluminum test piece was removed and the transducers were allowed to transmit signals in transmit-receive mode. Again, the transducers were adjusted, this time with the linear motors, until the amplitude reached a maximum value signifying that they were aligned. Because this particular setup was not altered during the course of the experiment, this alignment only needed to be performed once.

Shear speed of sound measurements could not be conducted with transmit-receive techniques similar to the longitudinal tests because water is incapable of transmitting shear waves; instead couplants with high viscosity are required for transmitting shear waves adequately. For this test, a single shear transducer with a shear ultrasonic couplant gel was used in pulse-echo mode to determine the speed of sound of the materials. A thin film of this gel was spread across one surface of each sample and the transducer was pressed down into the gel. Due to the lack of mechanical advantage for alignment, the finishing processes described earlier were assumed to be sufficient enough to align the transmitter with the back wall of the sample.

Imaging processes were also different for each type of speed of sound measurements. For the longitudinal mode, ten separate speed of sound signals were taken of each of the three faces of the geopolymer samples. These ten signals were taken at 1mm intervals along the geopolymer face. Due to the fact that a programmed linear motor was used to adjust the longitudinal samples, each A-line was only averaged 10 times to allow the signal to be captured before the motor began moving again. The shear mode was analyzed from only 5 A-lines from each sample taken at random locations on the face. However, because there were no time constraints on capturing the shear A-lines, each signal was averaged 100 times.

4.2.3 Characterization of Aluminum Test Piece

In order to qualify the robustness of the testing procedure, a plate of Mic-6(TM) aluminum produced by Alcoa was ground flat to a thickness of 0.5". This particular alloy is rated by its manufacturer for a modulus of elasticity of 71GPa [40]. Using the techniques described in this chapter, a value of 72.3GPa was determined for the elastic modulus. This percent error for this calculation is therefore 1.8% so that the overall procedure can be assumed to be accurate to within 2%.

Chapter 5

Results

5.1 Density and Porosity Analysis

5.1.1 Porosity Evaluation

Typical porosity evaluation techniques, such as nitrogen absorption or mercury intrusion, could not be performed for this study due to the lack of equipment and the hazards associated with handling mercury. Instead, a microscopy technique was applied to visually estimate the porosity contributions in each sample. This technique assumes that the pores are uniformly distributed throughout every sample. Each sample was ground flat with a surface grinder to smooth the surface and all rough edges and corners. Then a series of polishing wheels were used to further smooth the surface of each sample. Each sample was then viewed under an Olympus SZX12 stereomicroscope at 12.5x magnification. A digital camera mounted onto the microscope was used to capture three images from each set of samples so that it could be viewed on a computer using a software package provided by Olympus. This software was used to identify the circular pores and record their diameters onto the image. An example of these images is provided in figure 5.1. These diameters were then manually entered into a spreadsheet which would compute the average pore diameters, standard deviations in pore diameters, and the percent pore volume of each sample.

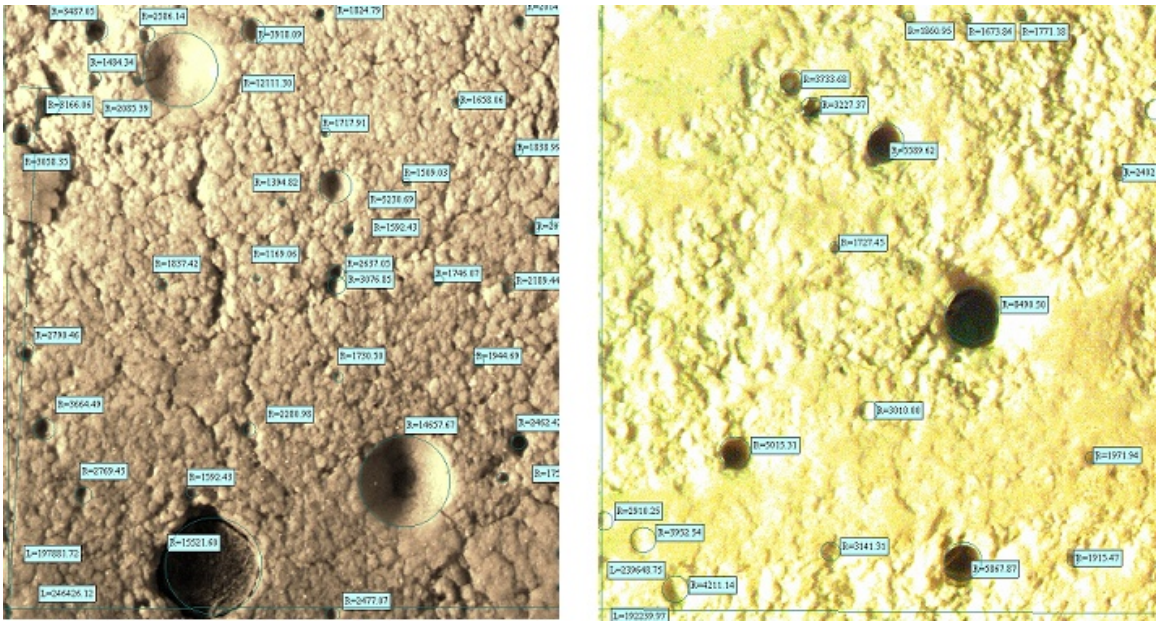

Figure 5.1: Microscopy images of geopolymer samples. The left panel shows an image of a 4.1 Si:Al sample while the right panel shows an image of a 1.9 Si:Al sample.

The pore diameter and percent pore volume data were evaluated as trends with the Si:Al ratios. These values are displayed in figure 5.2 and 5.3 respectively with exact values presented in table 5.1. The pore diameter and the percent pore volume both tend to decrease as the Si:Al ratio of the sample is decreased. However, the larger standard deviations in the 1.49 and 2.2 Si:Al ratio samples suggests that some of the pores present are due to entrapped air bubbles, which would be larger in diameter as opposed to those caused by unreacted materials or displaced water. This presence of entrapped air signifies that only 10 minutes of vibrating each sample may not be sufficient due to the differences in viscosity of the gel phase of each geopolymer batch.

Table 5.1: Averaged porosity data for each geopolymer sample set.

	1.49	1.52	1.9	2.2	3.1	4.1	6.4
% Pore Volume	4.66%	5.13%	3.58%	6.03%	2.87%	3.42%	3.53%
Average Pore Diameter (mm)	2.10	1.12	1.84	2.35	1.79	1.44	0.68
Standard Deviation of Pore Diameters (mm)	1.28	0.63	0.57	1.07	0.67	0.50	0.63

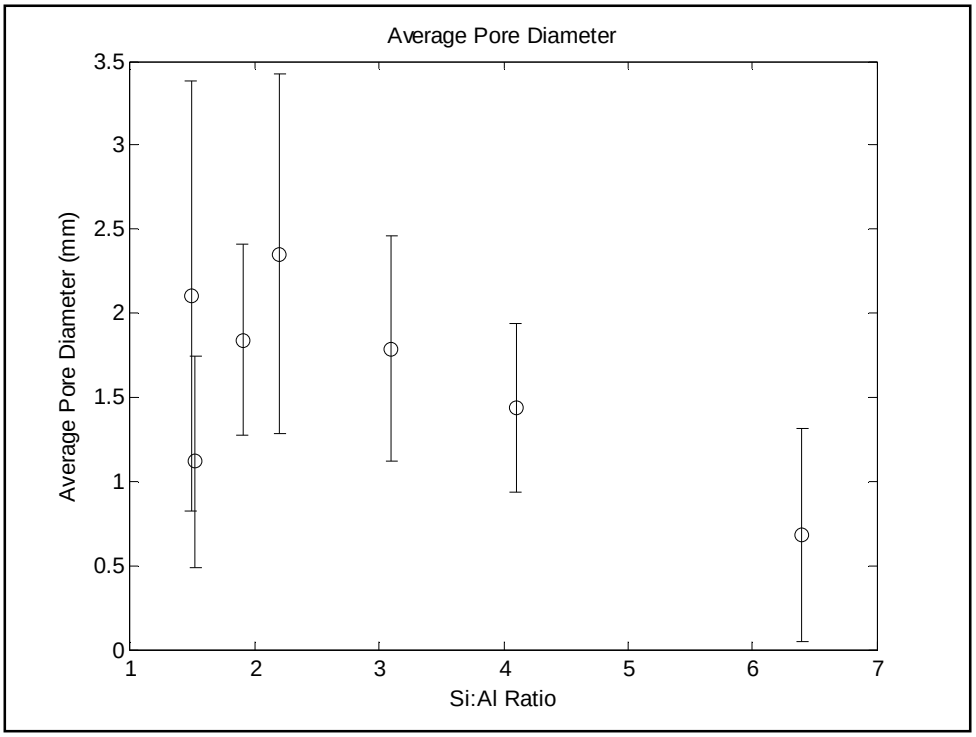

Figure 5.2: Average pore diameter with standard deviation of pore diameters for each Si:Al set.

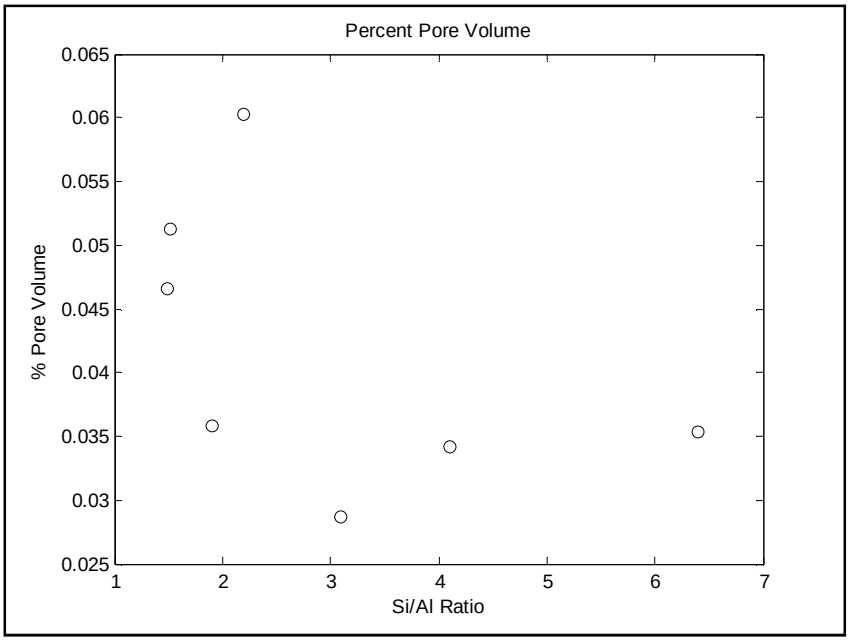

Figure 5.3: Percent pore volume for each Si:Al set.

5.1.2 Density Evaluation

Two different densities are discussed for each set of samples: sample density and binder density. The sample density is the overall density of the bulk material including vacancies from pores that were either trapped within the sample or created through the hydration process of geopolymerization. The sample density was determined using the Archimedean technique, with every sample being massed and then dropped into a water tank so that the displaced water could be measured with a graduated cylinder. This mass and volume measurement was then used to directly determine the density. Three samples from each set of Si:Al ratios were each measured three different times to gather a statistically significant data set. The samples were also dried and massed after

being removed from the water after each submersion to insure that they were not absorbing water which would affect the density measurements. In every case, there was no measurable difference in the mass of each sample

Since ultrasonic waves cannot be effectively transmitted through the pores a density of the geopolymeric binder is needed to evaluate the elastic properties of the material with this technique. Assuming that the mass of the materials trapped within the pores is negligible, the binder density can be calculated from the sample density and the percent pore volume by:

$$\rho_{Binder} = \frac{\rho_{Sample}}{1-(\%PV)} \tag{5.1}$$

Where ϱ is the density for both the binder and the sample and (%PV) is the percent pore volume of the sample. The binder and sample density for each sample set is presented in figure 5.4 and table 5.2

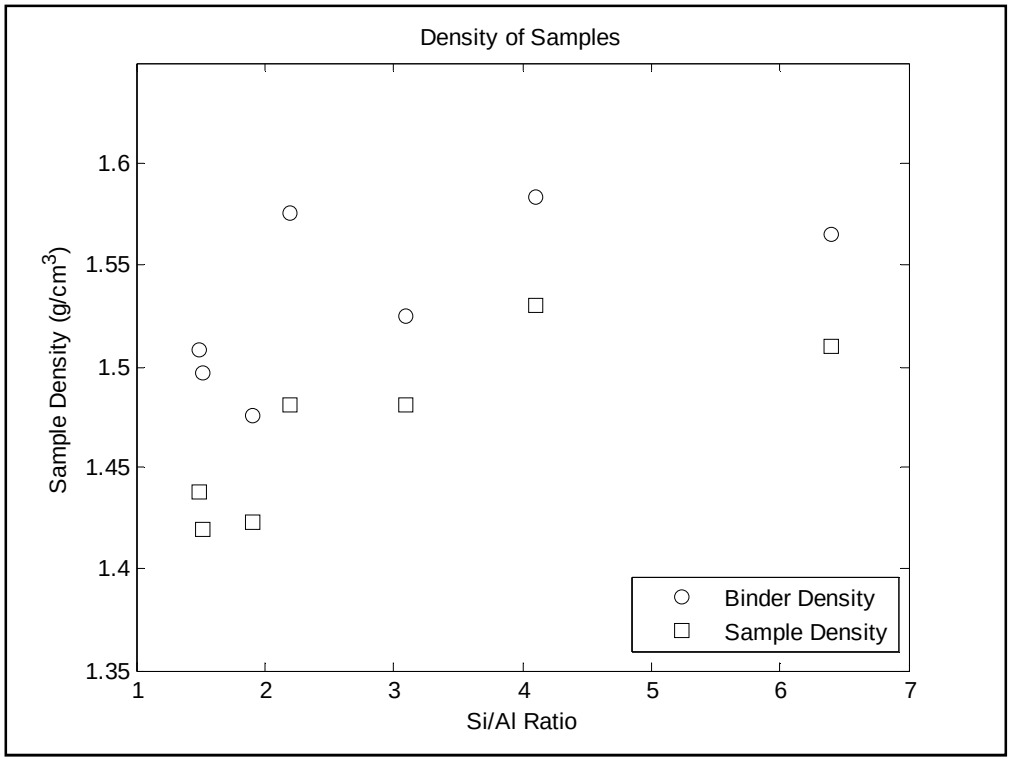

Figure 5.4: Comparison of densities of the samples and binders.

Table 5.2: Average binder and sample densities for each Si:Al set.

Si:Al Ratio	1.49	1.51	1.9	2.2	3.1	4.1	6.4
Sample Density (g-cm^{-1})	1438	1420	1423	1481	1481	1530	1510
Binder Density (g-cm^{-1})	1508	1497	1476	1576	1525	1584	1565

In each case, the binder density became higher than the sample density as was expected. The densities increase as the Si:Al ratio is increased until the 4.1 Si:Al sample after which the densities appear to remain constant. This increasing in density can be expected because as the Si:Al ratio is increased there will be a greater presence of Si-O-Si bonds as opposed to Si-O-Al bonds. Since the Si-O bond length is shorter that the Al-O bond length, the material should become more compact and therefore more dense. Similarly to the decrease in pore

diameter and percent pore volume, this could also be attributed to the geopolymerization being more complete with a greater concentration of the reactants being incorporated into the binder. Another explanation comes from Davidovits's theory that above the Si:Al ratio around 3, the geopolymer binder begins to take on the form of a PSDS structure in which there is a greater extent of Si-Si bonding within the geopolymer as opposed to the PSS structure, where $2 \leq Si:Al \leq 3$ and the primary bonding that occurs is Si-Al [1].

5.2 Acoustic Properties

5.2.1 Attenuation

No quantitative analysis for attenuation was performed in this study. Qualitatively however, it can be said that this material is highly attenuating making ultrasonic measuring sometimes difficult and making this type of material excellent for sound insulation. This qualitative analysis is based on the gain applied to the signal before capturing it. Gain, in this sense is increasing the amplitude of the signal by some multiplier. Gain can be either positive or negative depending on whether the peaks of the signal need to be increased to be visible or gain can be negative if the amplitude of a signal is higher than the limit of the oscilloscope and is clipped.

As a reference, when analyzing signals transmitted through the aluminum test piece, a range of -7dB to -8dB was used and when analyzing signals sent directly through water a gain of -1.7dB was used. For the longitudinal measurements of the geopolymer samples, the typical gain needed increased as the Si:Al ratio increased. The average gain for each sample is presented in table 5.3. While it may be tempting to see these two sets of data and assume that the longitudinal mode had a higher attenuation than the shear mode, this assumption would be ill founded because the thickness used for the longitudinal samples was nearly 500% that of the shear samples meaning that there was much more material to dissipate the energy for the longitudinal ones. However, the shear signals, when amplified with a similar gain, would introduce too much extra noise and the signal could not be discerned so each sample was ground until it was thin enough that a signal could penetrate it with a similar amount of gain. It is worth noting however that the gain used in the 6.4 Si:Al ratio sample was significantly higher than every other sample signifying that this sample would have a higher attenuation coefficient.

Table 5.3 Average gains used when analyzing signals for each Si:Al set.

Si:Al Ratio:	1.49	1.52	1.9	2.2	3.1	4.1	6.4
Gain for Shear Mode (+dB)	0.3	0.6	0.8	0.5	0.4	0.5	3.0
Gain for Longitudinal Mode (+dB)	3.0	3.0	3.6	3.5	3.0	3.3	5.1

5.2.2 Justification of Isotropic Assumption

In order to justify the assumption that the geopolymer samples behave isotropically, the average group velocity for the x, y, and z directions discussed in section 4.1.3 were determined for each sample. If the average group speed for each direction were similar for each sample in both the longitudinal and shear modes, then it can be assumed that the elastic properties would also be equivalent. As can be seen in figure 5.5, the speeds of sound for the longitudinal direction are all very similar with the exception of the 6.4 Si:Al ratio sample whose differences can be attributed to the high attenuation which was discussed earlier. The shear speed of sound, shown in figure 5.6, were not as nicely clustered as they were in the longitudinal case, but there is no sign that any one direction is experiencing any significant deviations compared to the others. Therefore, when analyzing the elastic properties, it can be safely assumed that the material is behaving isotropically and all of the data for each sample set will be used when determining the average speed of sound.

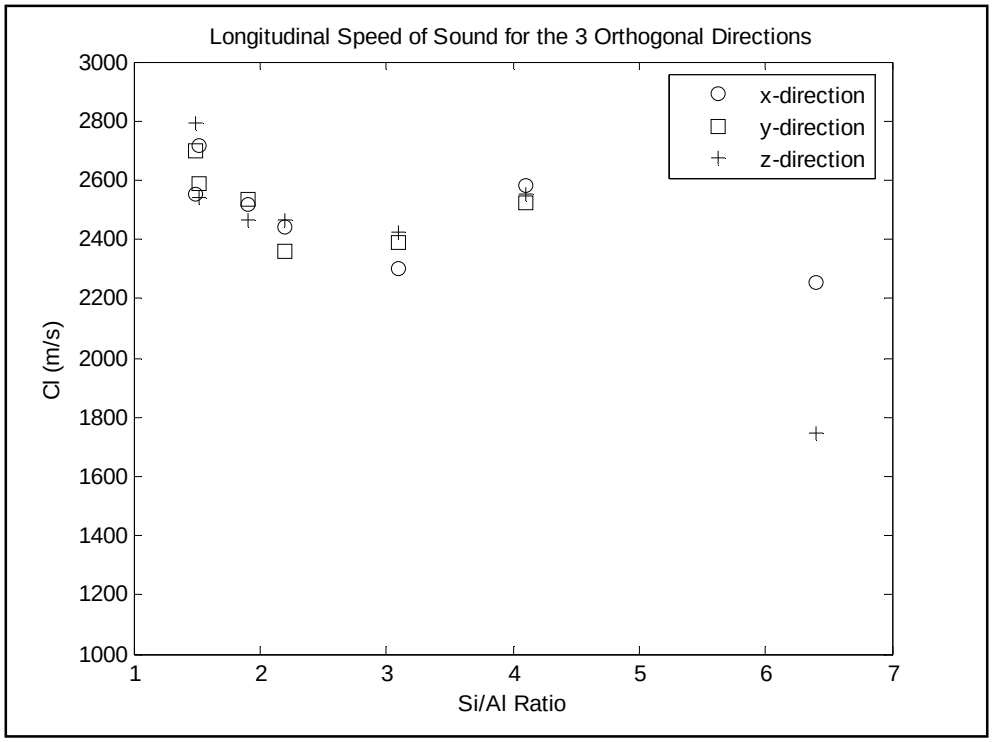

Figure 5.5: Speed of sound of the longitudinal mode for each of the orthogonal directions for each Si:Al set.

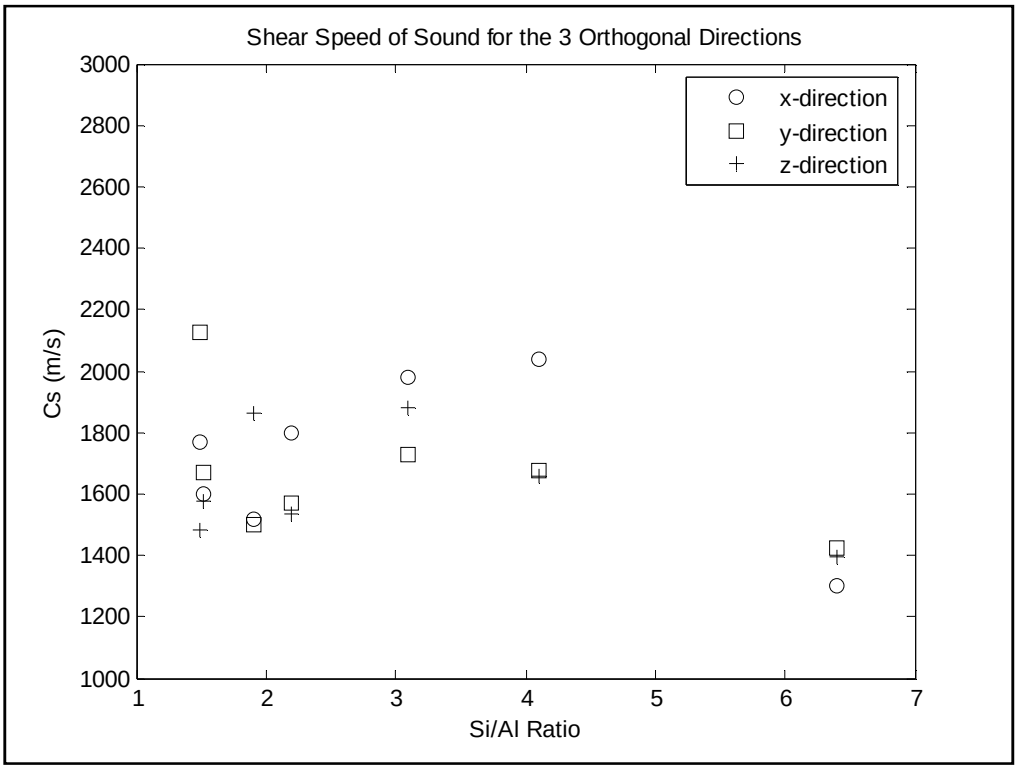

Figure 5.6: Speed of sound of the shear mode for each of the orthogonal directions for each Si:Al set.

5.2.3 Speed of Sound

The average group velocities for both the longitudinal and shear modes were calculated for each geopolymer sample set. These speed of sound measurements along with the computed errors are shown in figure 5.7 and table 5.4. These show that within the PSS range with Si:Al ratios between 1.49 and 3.1, the shear speed of sound velocities remain relatively constant while the longitudinal velocities gradually decrease with increasing Si:Al ratio. The two samples in the PSDS range, with 4.1 and 6.4 Si:Al ratios, show much lower speed of sounds than the lower Si:Al ratios. There is an increase in the speed of sound for both the longitudinal and shear modes in this region as well, but there is not enough data to conclusively support this as a trend.

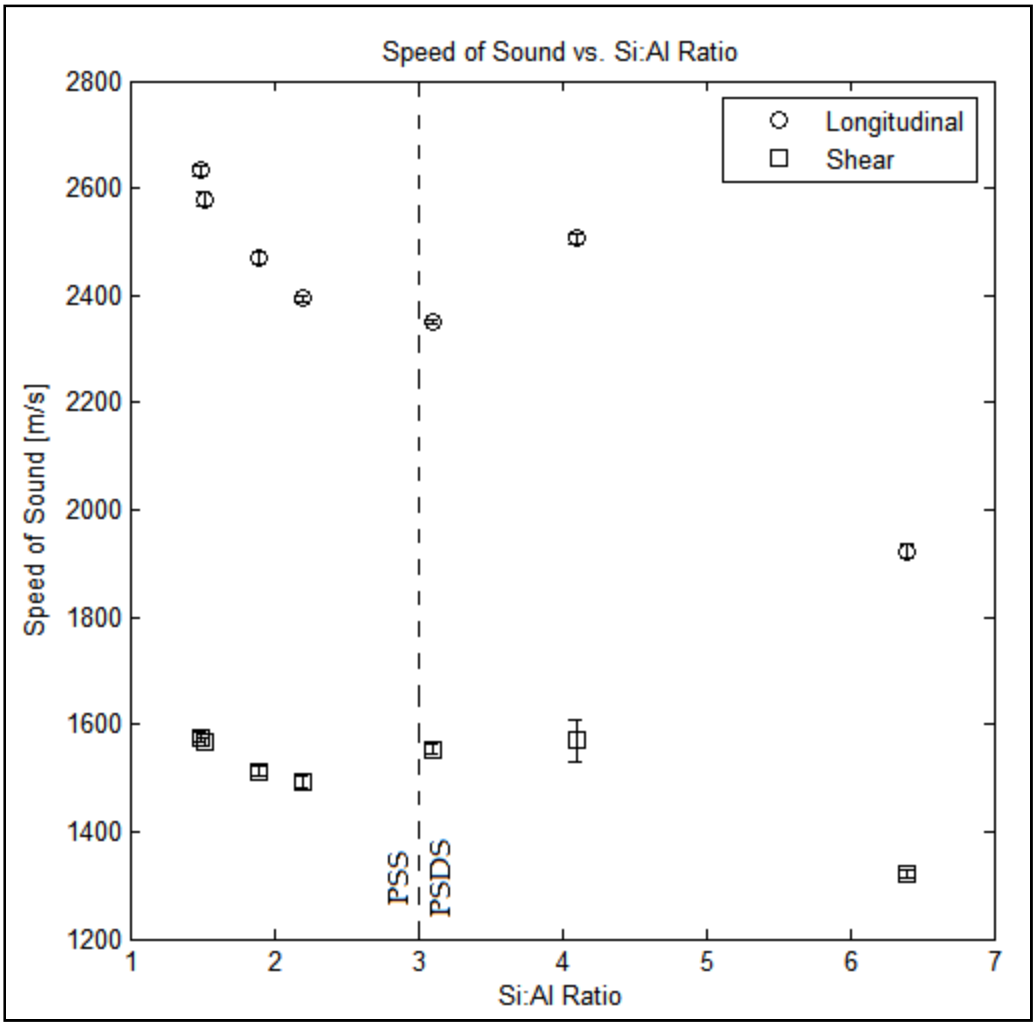

Figure 5.7: Average speed of sound measurements for each Si:Al set.

Table 5.4: Average speed of sound measurements for each Si:Al set.

Si:Al Ratio	1.49	1.52	1.9	2.2	3.1	4.1	6.4
Longitudinal Velocity [m/s]	2632.3	2579.5	2469.2	2393.6	2350.0	1884.1	1923.1
Longitudinal Standard Deviation [m/s]	8.05	11.85	11.48	6.45	4.09	8.82	11.77
Shear Velocity [m/s]	1575.4	1566.7	1513.1	1494.3	1554.2	1156.6	1321
Shear Velocity Standard Deviation [m/s]	9.53	8.52	10.81	10.88	11.05	38.87	6.42

5.3 Elastic Properties

5.3.1 Elastic Modulus

The shear and longitudinal speeds of sound were used to directly determine the elastic modulus for each set of geopolymers and are presented here in table 5.5. Since the chemical reactions during geopolymerization that affect the elastic modulus also affect the other physical characteristics of the samples, the elastic modulus was compared to the binder density, sample density, average pore diameter and percent pore volume determined for each sample set. Plots of the elastic modulus with respect to each of these characteristics are presented in figures 5.8-5.12.

Table 5.5: Elastic modulus for each Si:Al set.

Si:Al Ratio:	1.49	1.52	1.9	2.2	3.1	4.1	6.4
Elastic Modulus [GPa]	9.14	8.87	8.11	8.31	8.19	5.08	5.75
Standard Deviation [GPa]	0.172	0.245	0.164	0.273	0.180	0.311	0.112

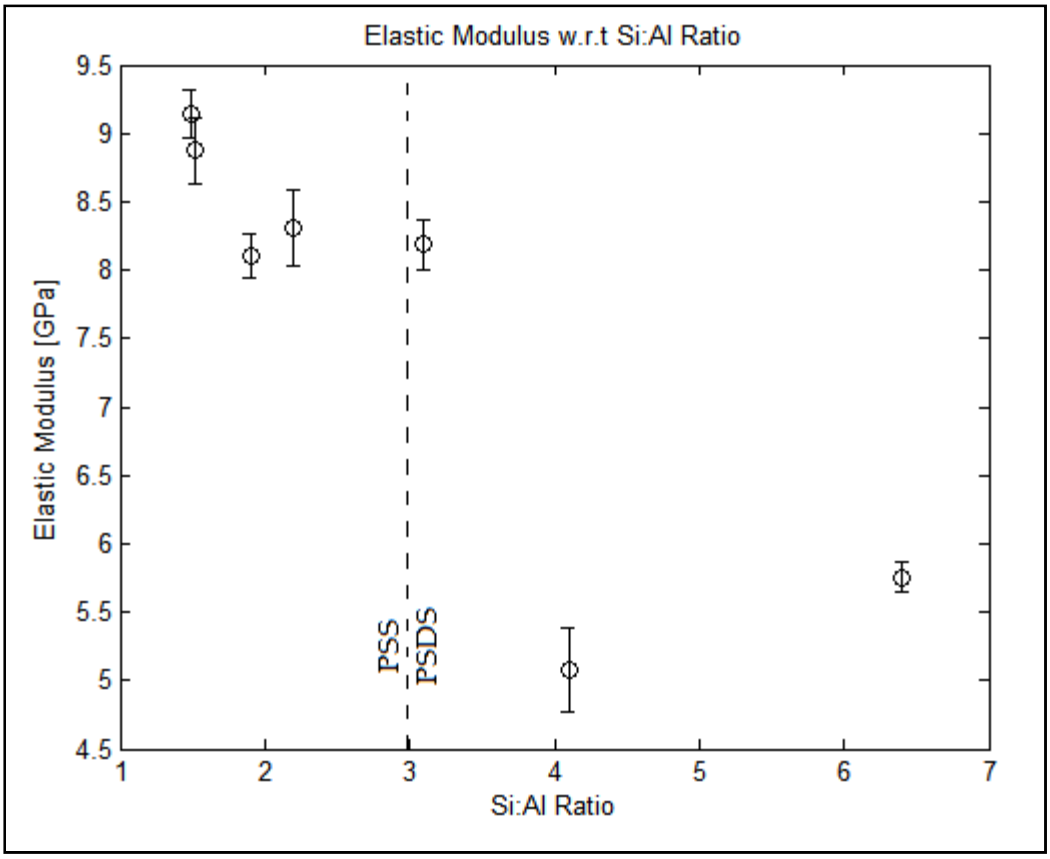

Figure 5.8: Elastic modulus of each sample plotted with respect to the Si:Al ratio.

The elastic modulus remains relatively similar with values between 8GPa and 9GPa for the first five samples when compared to the Si:Al ratio. Then, for the two highest Si:Al samples the elastic modulus drops down to a value around 5GPa. This effect of a sudden change in properties near the Si:Al=3 point further suggests that the change in elastic properties is directly related to the changing between PSS and PSDS formations discussed by Davidovits [1]. The reason for the 3.1 Si:Al sample appearing to behave like a PSS sample while lying in the PSDS range is that the Si:Al ratios presented in this study are all theoretical ratios. It is likely that there is some amount of unreacted material in each sample.

Therefore, the 3.1 Si:Al sample is most likely still a PSS geopolymer even though it has a Si:Al ratio above 3.

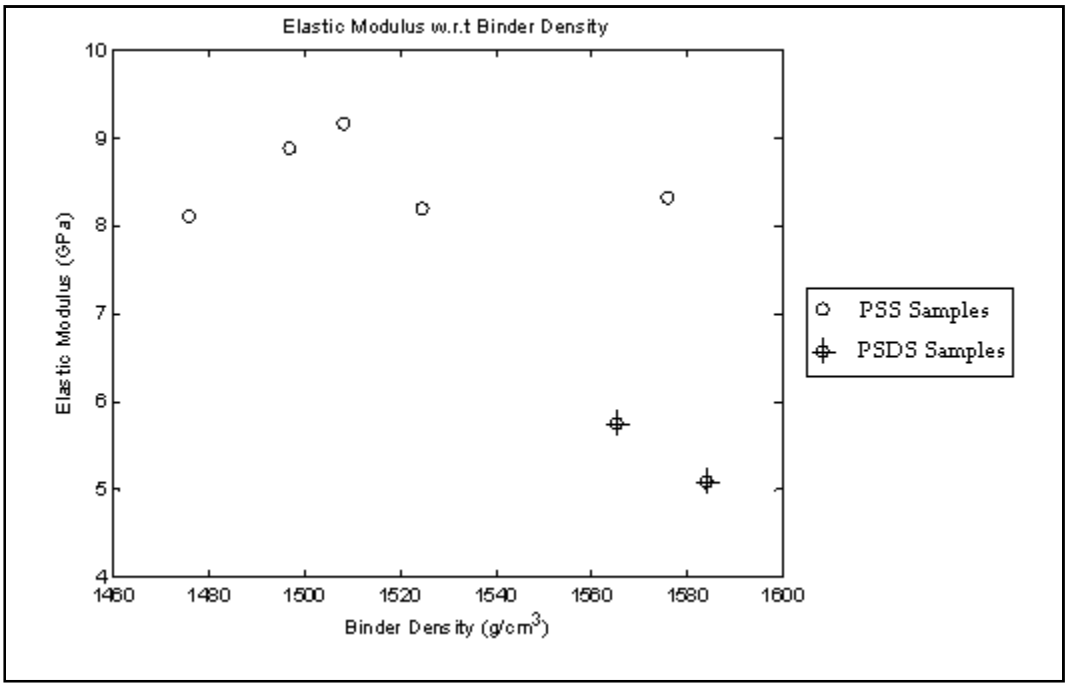

Figure 5.9: Elastic modulus of each sample plotted with respect to the binder density.

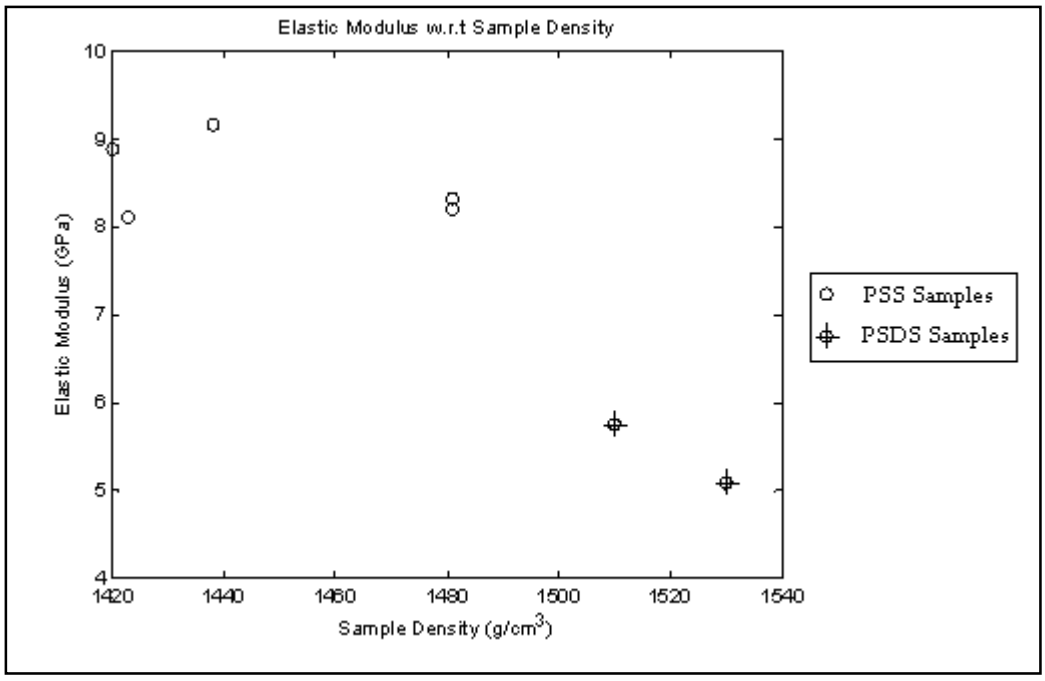

Figure 5.10: Elastic modulus of each sample plotted with respect to the sample density.

An inverse relationship can be seen when the elastic modulus is compared to the binder and sample densities in figures 5.9 and 5.10 respectively. This trend implies that an increase of the Si-O-Si bonds within the binder with an increase in the Si:Al ratio will cause the material to become simultaneously more dense while also allowing it to be more compliant. This can also be attributed to the fact that as the average pore diameter decreases, the density tends to increase. Smaller pores would allow the material to deform more because there will be fewer voids which cannot support the elastic deformations analyzed here.

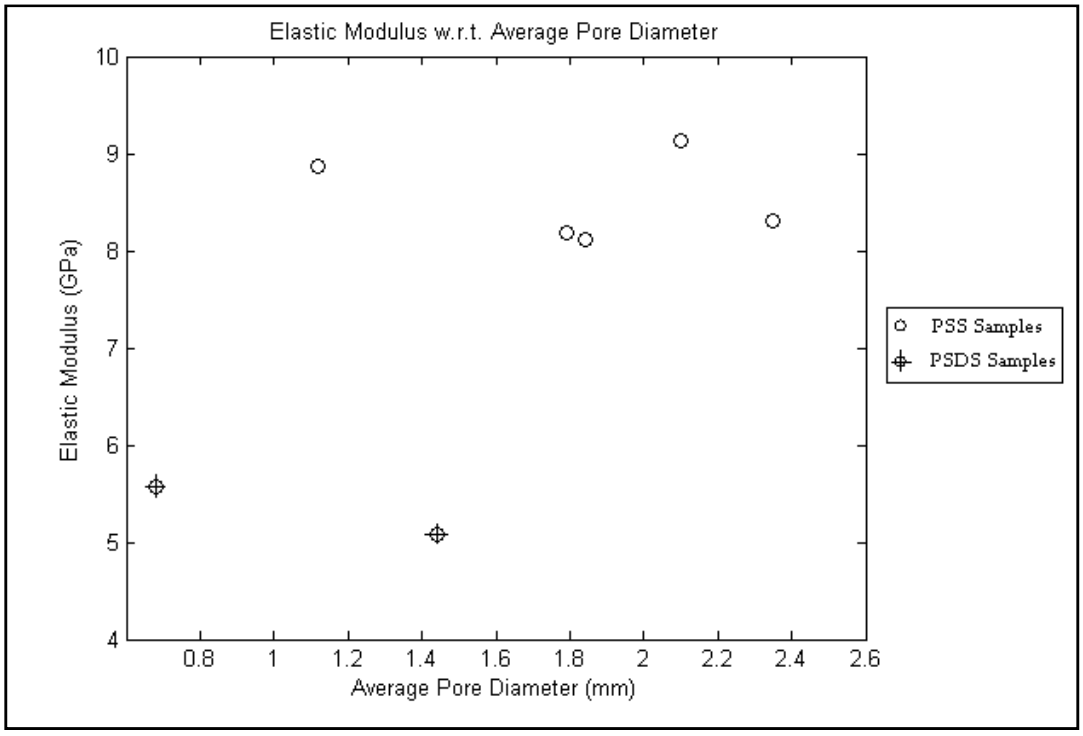

Figure 5.11: Elastic modulus of each sample plotted with respect to the average pore diameter.

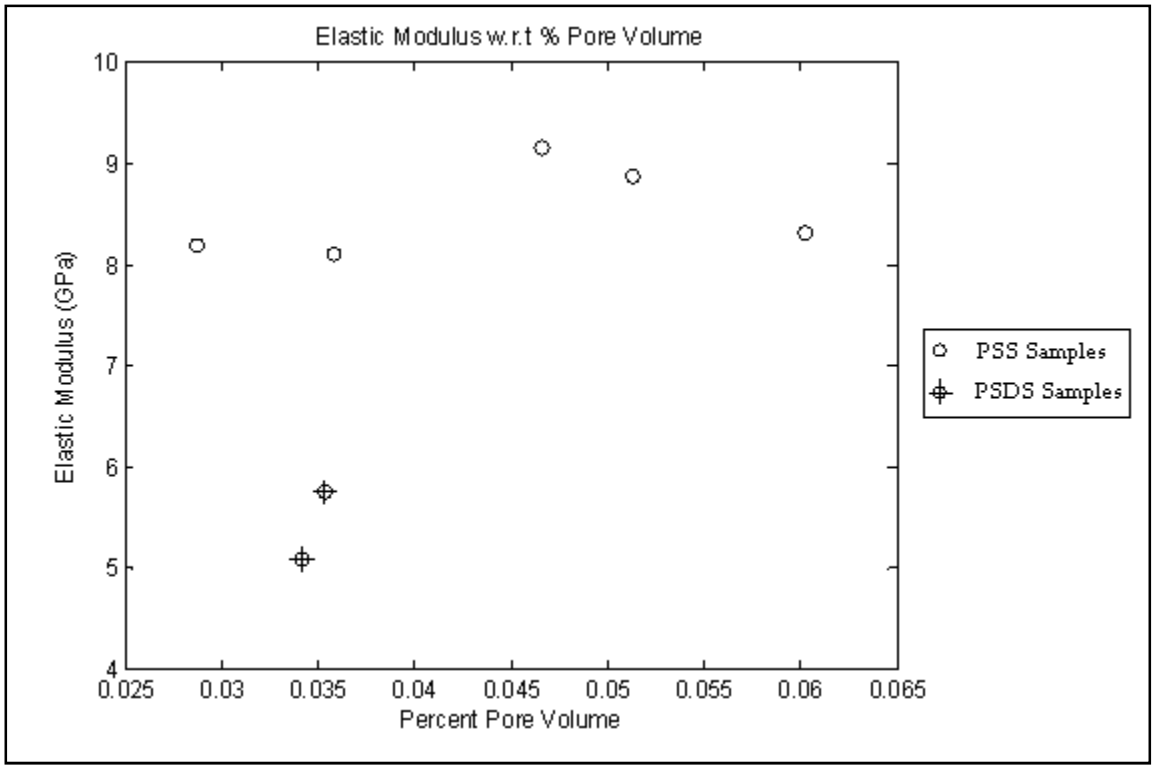

Figure 5.12: Elastic modulus of each sample plotted with respect to percent pore volume.

The relationship between the elastic modulus and the porosity measurements did not demonstrate a strong correlation. As was discussed earlier, smaller pore diameters and larger percent pore volumes did allow for a lower elastic modulus, meaning that the material as a whole was more flexible. However, it is still likely that entrapped air pockets within the binder are responsible for less accurate measurements of the porosity in some samples compared to others making any trends difficult to determine.

5.3.2 Poisson's Ratio

Poisson's ratio was also established directly from the shear and longitudinal values for the speed of sound. The values determined, given directly in table 5.6, were also compared to the Si:Al chemical ratio as well as the physical characteristics of the samples as are displayed in figures 5.13-5.18 so as to determine which properties of the materials are related.

Table 5.6: Poisson's ratio for each Si:Al sample set.

Si:Al Ratio:	1.49	1.52	1.9	2.2	3.1	4.1	6.4
Poisson's Ratio	0.221	0.208	0.199	0.181	0.111	0.198	0.053
Standard Deviation	0.003	0.003	0.003	0.003	0.002	0.010	0.001

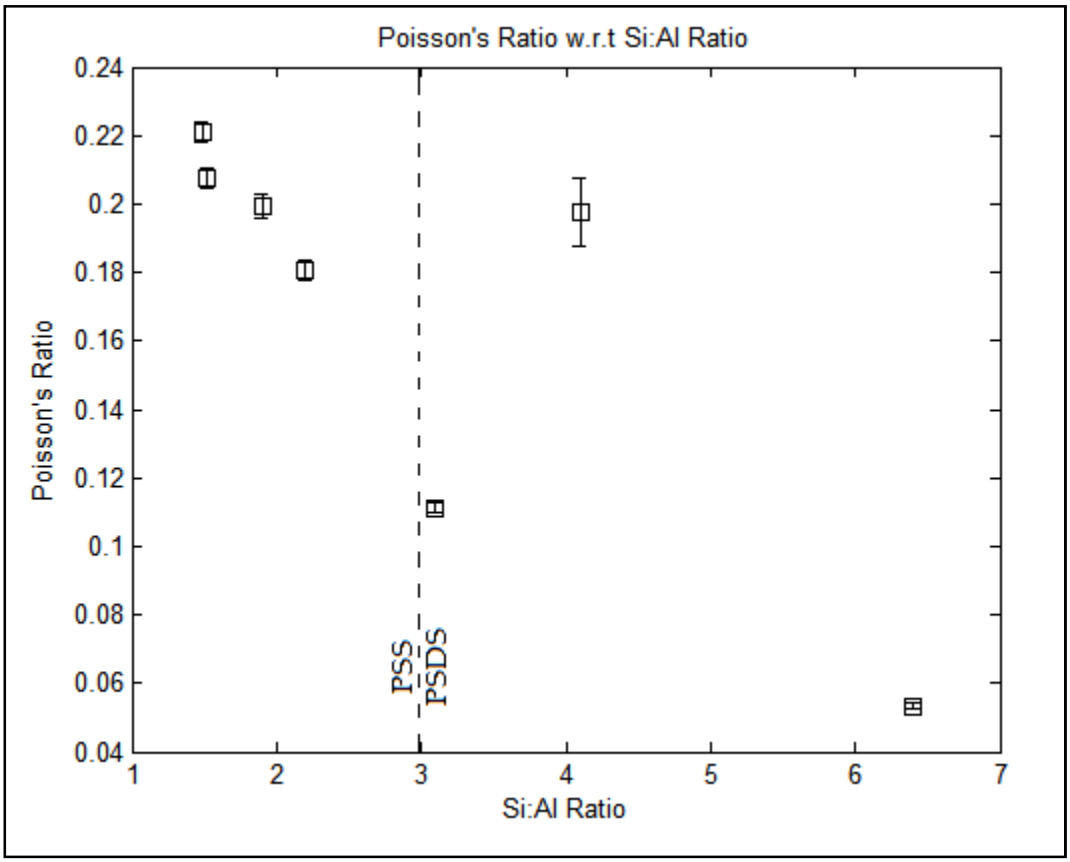

Figure 5.13: Poisson's ratio of each sample plotted with respect to the Si:Al ratio.

The Poisson's ratio has a general trend of decreasing as the Si:Al ratio is increased with the exception of a peak at the Si:Al=4.1 point. Therefore, as the Si:Al ratio increases the geopolymers will become progressively more brittle within the PSS range. The peak at Si:Al equal to 4.1 again shows that there is a changing of properties at the PSS and PSDS transition point. However, the Poisson's ratio for the 6.4 Si:Al sample is conspicuously low with a value near 0.05. This sample is indeed very brittle, but this value is much lower than expected and may be due, in part, to poor data collected because of its high attenuation.

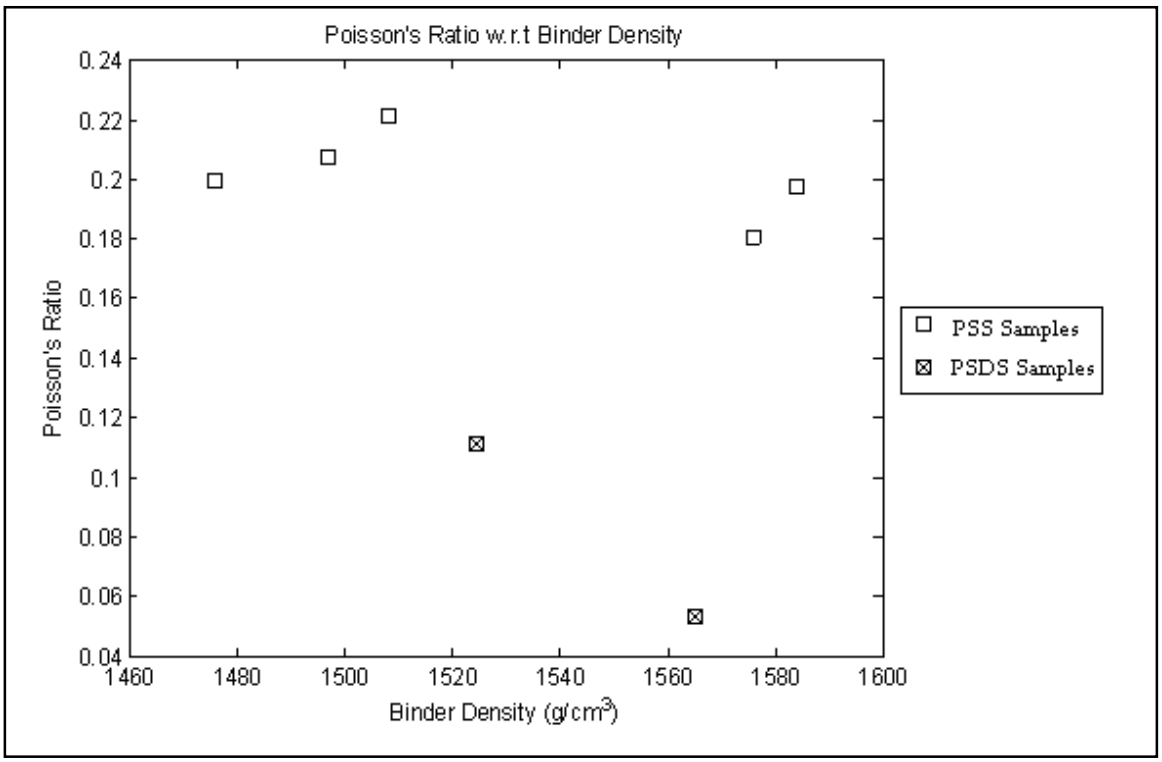

Figure 5.14: Poisson's ratio of each sample plotted with respect to the binder density.

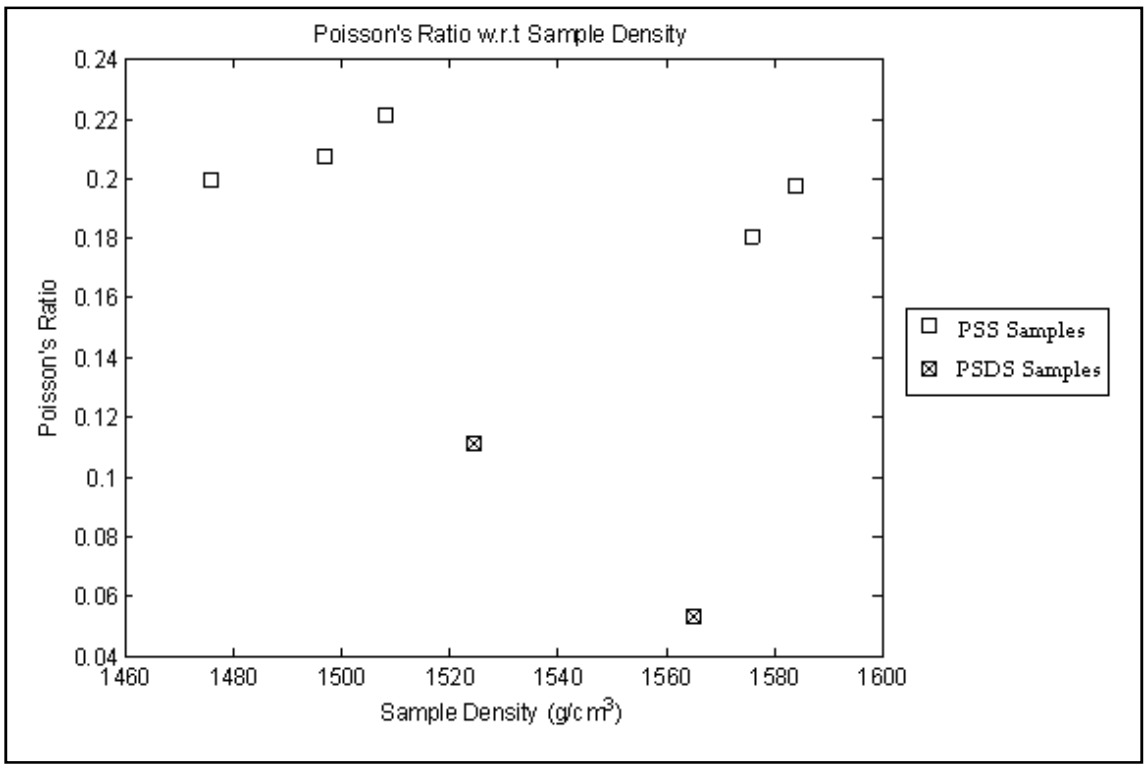

Figure 5.15: Poisson's ratio of each sample plotted with respect to the sample density.

The Poisson's ratio is not highly dependent upon either density of the material. The equation used to derive the Poisson's ratio from the speed of sound had no density variable in it so it is not surprising that no correlation is present in either figures 5.14 or 5.15.

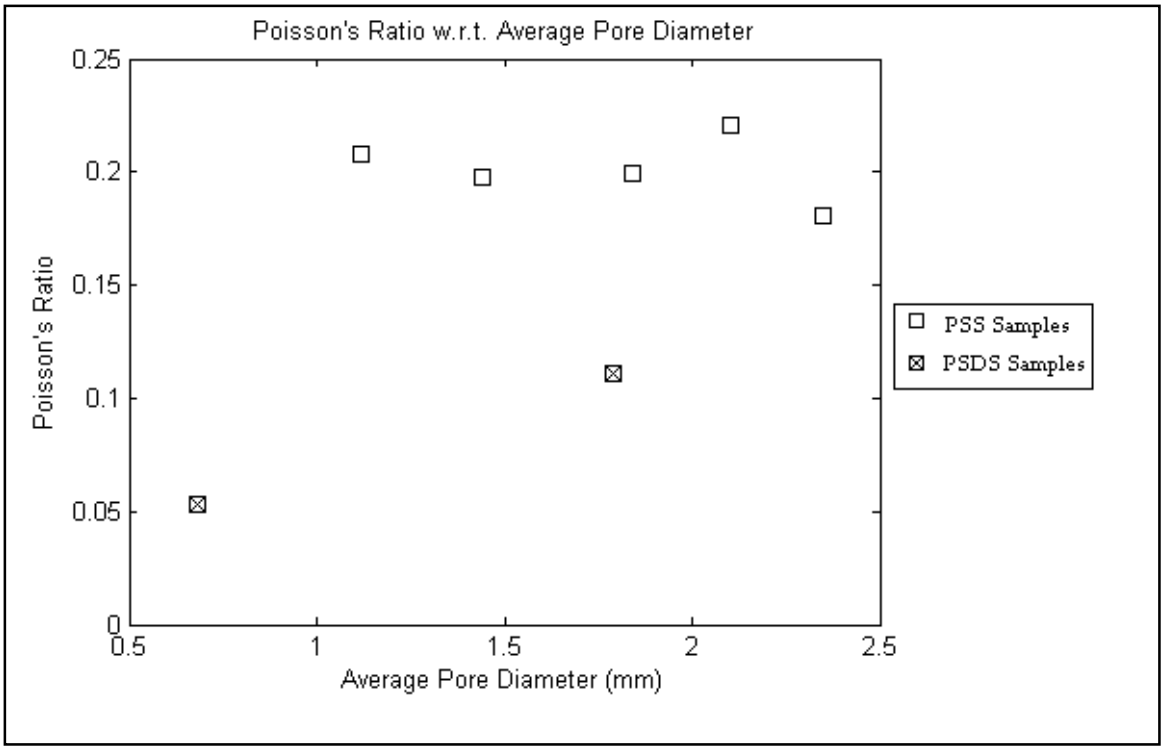

Figure 5.16: Poisson's ratio of each sample plotted with respect to the average pore diameter.

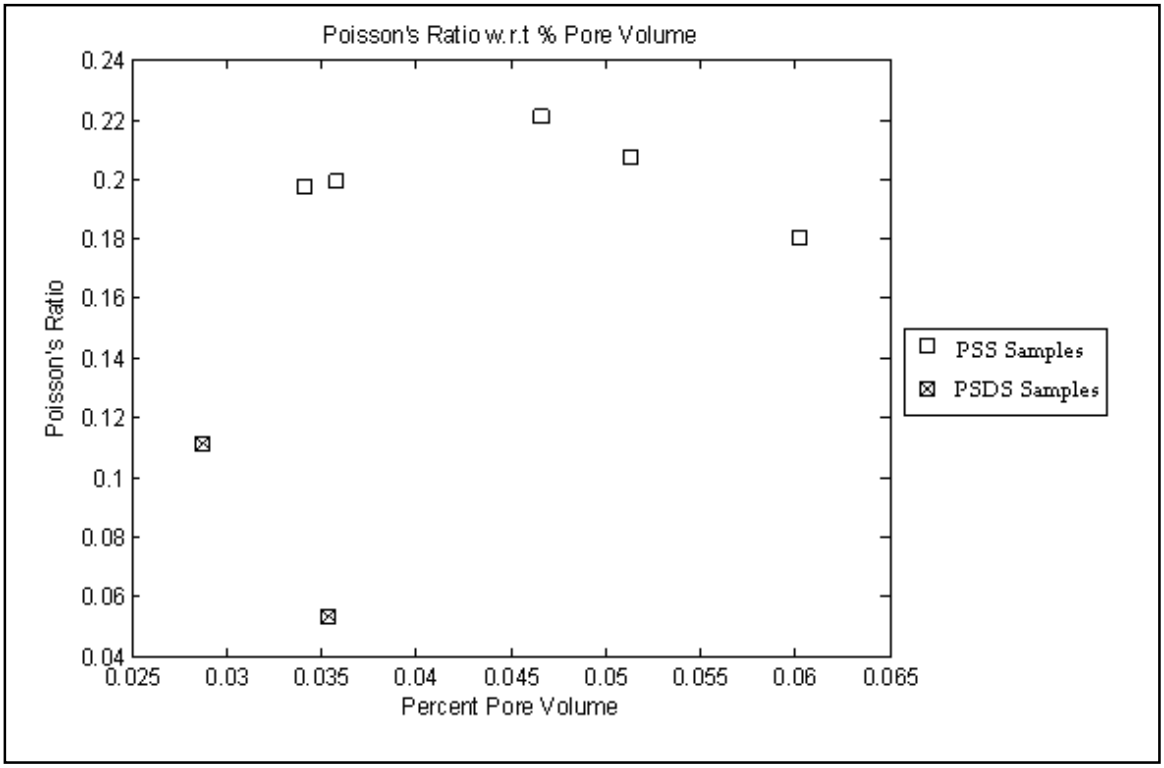

Figure 5.17: Poisson's ratio of each sample plotted with respect to the percent pore volume.

Similar to the density measurements, the porosity measurements also appear to have no effect on the Poisson's ratio. As the Poisson's ratio decreases, the binder can be said to become more brittle. The presence of pores within the material should have no impact on how brittle the binder is making the lack of a correlation expected.

Chapter 6

Infrared Characterization

Infrared absorbtion spectroscopy involves the exposing a sample to polychromatic electromagnetic radiation, and measuring the absorption of this radiation [45]. As the name would imply, the range of wavenumbers of this radiation spans the infrared spectrum from $10cm^{-1}$ to $14000cm^{-1}$. As this radiation strikes the sample, if the energy of the radiation is equal to the energy difference between two of the quantum excited states, then the energy of the photon will be absorbed so as to transition the energy level of the molecule to a higher state [46]. For example, if a molecule at some ground energy level, E_0, is struck by an infrared photon with some resonant energy of the bond, E_{IR}, then the molecule will be transitioned to a higher energy level, E_1, according to the De Broglie relation:

$$E_1 - E_0 = E_{IR} = \hbar\omega_{IR} \tag{6.1}$$

Where ω_{IR} is the frequency of the infrared photon and ħ is Dirac's constant.

The infrared spectra bands will originate due to four main types of resonances of the molecular structure. These four modes of vibrations are stretching, in-plane bending, out-of-plane bending, and torsion. Typically, the frequencies associated with each of these types modes of vibration will be found at progressively lower frequencies in respect to the order presented here [45].

Infrared analysis was performed on each geopolymer sample as well as the source metakaolin using a Bio Rad Excalibur Series FTS 3000 infrared

spectrometer along with the Digilab Merlin software package to analyze the spectra. Absorbance data collected for these samples, shown together in figure 6.1, was compared to known values of vibration spectra for similar materials. A synopsis of the characteristic infrared vibrational bands for class F fly ash, which is composed of similar materials, was produced and provided in table 6.1.

Table 6.1: Characteristic IR Vibrational Bands of class F fly ash [41].

Mode of Vibration	Associated Bonds	Wavenumber (cm^{-1})
asymmetric stretching	Si-O-Si Al-O-Si	950-1250
Stretching	$Si\text{-}O^{-}R^{+}$	950-980
Si-O streching with OH bending	Si-OH	882
symmetric stretching	Si-O-Si	798
symmetric stretching	Si-O-Si Al-O-Si	727
symmetric stretching	Si-O-Si Al-O-Si	620
symmetric stretching	Al-O-Si	561
Bending	Si-O-Si Al-O-Si	466

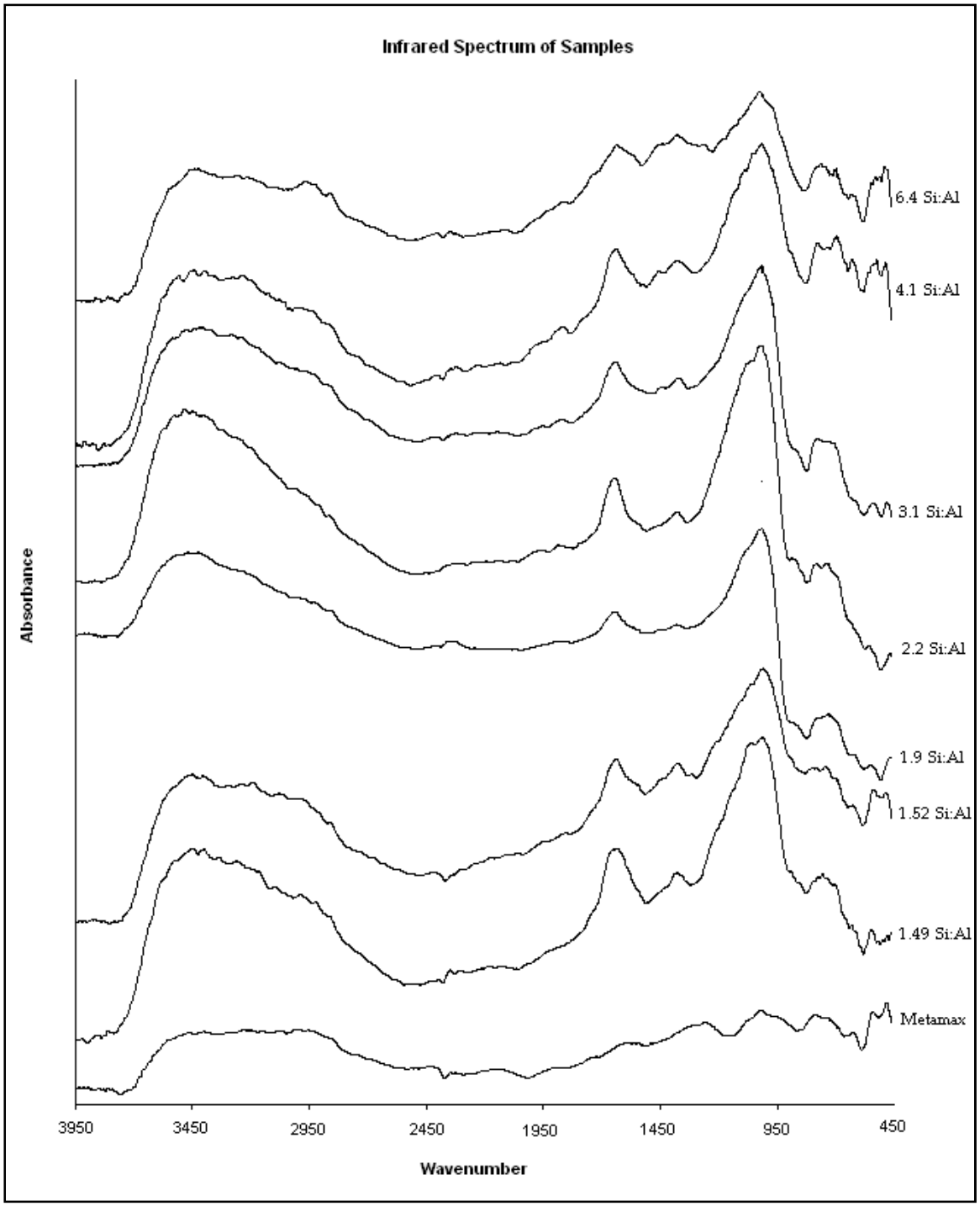

Figure 6.1: Infrared spectra of the seven geopolymer samples along with the metakaolin used as an activating ingredient.

The material structures could then be inferred from this comparison. Early investigations into the chemical structure of geopolymers proposed that the

tetrahedral alumina and silica join together in a sodalite structure, such as the one shown in figure 6.2. The infrared absorbance spectrum of a sodalite network with the chemical formula $Na_4Al_3Si_3O_{12}Cl$ is expected to have peaks at wavelengths 438cm^{-1}, 466 cm^{-1}, 670 cm^{-1}, 712 cm^{-1}, 737 cm^{-1}, 980 cm^{-1}, and 1020 cm^{-1} as can be seen in figure 6.3

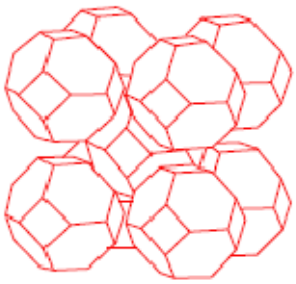

Figure 6.2: Diagram of a typical sodalite structure.

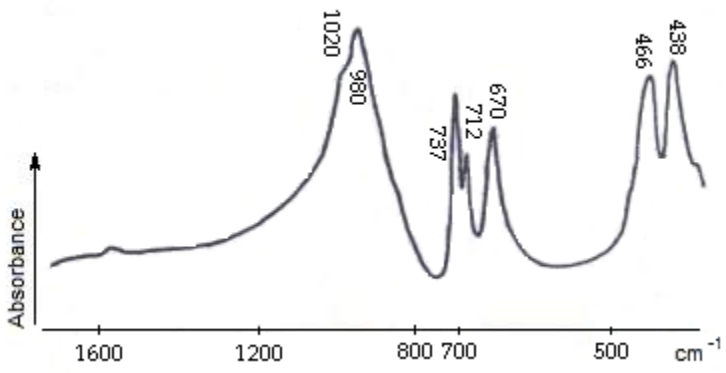

Figure 6.3: Infrared spectra of Sodalite with Chlorine [42]

The sodalite structure for geopolymers is different however in that the chlorine anion present in the given structure for sodalite is replaced with a hydroxide anion. It is expected that the asymmetrical stretching of the Al-O or Si-O bonds corresponding to the peaks at 980cm^{-1} and 1020cm^{-1} will not vary due to

changing the anion; however previous research has shown that a smaller anion will produce an upward shift of the lower peaks [43]. The location of the expected peak values for a sodalite structure with chlorine is marked with vertical lines overlaid on the spectra for the 8 samples presented earlier and shown in figure 6.4. While adequate resolution for the lower wave numbers was not possible with the equipment used in this study, it can be clearly seen that the principle peak are indeed uniformly shifted by approximately $50cm^{-1}$.

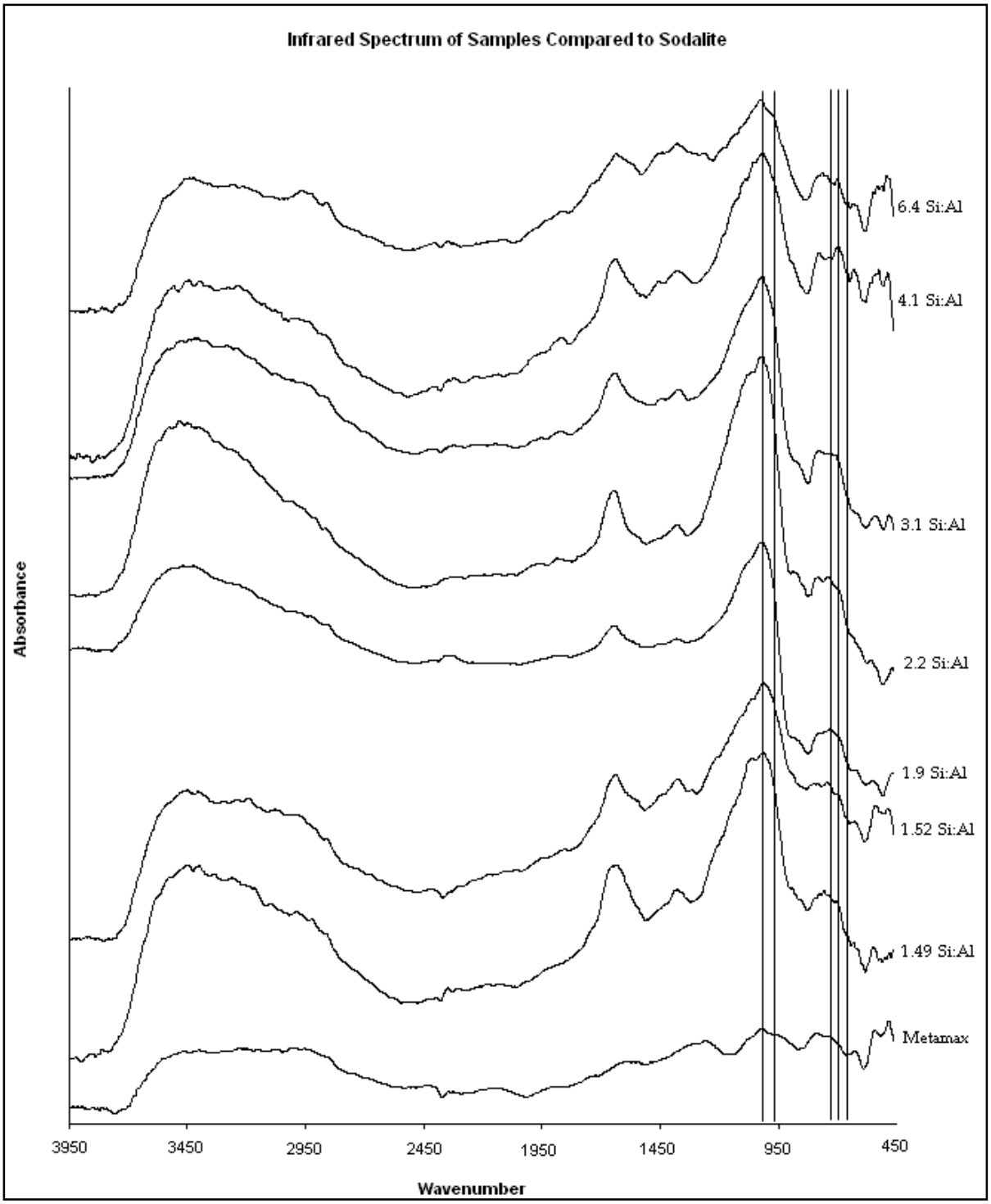

Figure 6.4: Infrared spectra of geopolymer samples compared to the peak positions of sodalite with chlorine.

While a shifting of the lower peaks was expected as a result of using a smaller anion, the shifting of the two peaks near 980 cm^{-1} and 1020 cm^{-1} cannot be

explained similarly. This shift of the asymmetric stretching vibration of the T-O-Si bond, where T represents either Si or Al, was theorized in one study to be due to the effect of incomplete dissolution of the alumina and silica [44]. When alkali is added to the alumniosilcate source materials, the oxygens in the alumina and silica tetrahedrons will bond less often leaving these structures more isolated [44]. This will in turn cause the vibrational bond to shift towards lower wave numbers [44]. This method can then be applied to determine the amount of alumina and silica added to the binder that was reacted and available for geopolymerization. The relationship between depolymerized aluminosilicates and shift in vibrational band was found to be linear with 100% crystalinity corresponding to a peak at 1068cm^{-1} and purely amorphous state corresponding to a peak at 1010cm^{-1}. The principle peak for the samples evaluated for this study were consistently near 1040 cm^{-1} meaning that each sample reacted evenly compared to each other and included approximately 75% of the included materials according to [44]. This cannot definitively determine the actual Si:Al binder for each sample because there is no differentiation between the reacted silica and alumina. However, this test does show that the theoretical Si:Al ratios provided in this study are sufficient in distinguishing between each sample set and that each sample set had a similar degree of reaction.

Chapter 7

Conclusions and Suggestions for Future Work

7.1 Conclusions

This study focuses on the non-destructive testing of geopolymers using ultrasonic techniques with intent to classify the mechanical properties. In addition to evaluating the elastic modulus and Poisson's ratio, porosity and density analysis were also performed. Based on the results discussed in the preceding chapters, the following conclusions have been made:

1. The geopolymer samples may be considered isotropic with regards to their elastic properties. This implies that the porosities are aligned randomly and are evenly distributed throughout the geopolymer binder.
2. The elastic modulus has an inverse linear relationship to the Si:Al ratio in the PSS range for Si:Al ratios spanning from around 1.0 to 3.0. Within this range of samples the evaluated elastic modulus range from 8.1 to 9.1GPa After this point, the geopolymers enter into the PSDS range where the elastic modulus sharply drops to around 5.5GPa.
3. Within the PSS range of Si:Al ratios, the Poisson's ratio decreased with increasing Si:Al ratio. There was a clear discontinuity in this trend with higher Si:Al ratio samples within the PSDS range.
4. As the Si:Al ratio is increased, the geopolymer will experience an increase in density with a decrease in the average pore size.

5. Geopolymers have shown themselves to be excellent sound insulators. While this makes ultrasonic testing difficult at times, it presents this type of material for a variety of applications involving noise and vibration damping.
6. The speed of sound can be determined roughly from the Si:Al ratio of the sample. While in the PSS range, the longitudinal speed of sound decreases from 2630 ms^{-1} to 2350 ms^{-1} while the shear speed of sound remains constant around 1500 ms^{-1}. In the PSDS range the speed of sound is around 1900 ms^{-1} for longitudinal waves and 1200 ms^{-1} for shear waves.

7.2 Suggestions for Future Work

1. A definite change in properties was observed as the geopolymer sample transitioned from the PSS range to the PSDS range. However, there were not enough samples in the PSDS range to effectively study what sort of trends can be expected. Using a similar approach to determine the elastic properties of geopolymers in the PSDS range would be a beneficial study.
2. This research focused on the effect of altering only one variable. Studying the effects of other variables including the curing regiment, alkali activating solution, and water content would also be useful studies. Ideally, it would be useful to have developed enough data so that the

properties of a geopolymer could be accurately predicted from knowing all of the elements going into making the geopolymer.

3. Ultrasonic testing could be performed to determine the elastic property of a sample not only after it has set but also while it is in the process of setting. Using this technique, the rate of solidification over time could be determined using ultrasonic techniques to provide a greater understanding of the geopolymerization process.
4. Attenuation has been shown to be a function of both absorption and scattering effects. If an ultrasonic transducer with higher signal amplitude could be used in pulse echo mode, it may be possible to develop a test to determine the porosity as well as the elastic properties of a sample with only one scan

Appendix A: Sample Compositions

Table A.1: Chemical constituents for geopolymer samples.

Sample Si:Al	1.49	1.52	1.9	2.2	3.1	4.1	6.4
NaOH (g)	60	60	60	60	60	60	64
H_2O (g)	100	100	100	100	100	100	101
Sodium Silicate (g)	320	320	320	320	320	320	320
Metamax (g)	470	440	390	370	300	300	150
Amorphous silica (g)	0	0	55	120	200	350	300

Appendix B: Development of Amorphous Alumina

In an effort to create geopolymer samples with Si:Al ratios lower than 1.49 while maintaining the water ratio used in this experiment, two attempts to calcinate alumina so as to alter it into its amorphous state were attempted. It has been suggested that the only 2 hours of calcination at 750°C is required to effectively alter raw kaolin into metakaolin [7]. It is therefore plausible that a octahedral aluminum may be capable of being transformed into tetrahedral aluminum within a similar time frame. Two experiments were performed to validate this assumption using alumina purchased from Fisher scientific and kilns provided by the Ceramics Department of the College of Imaging Arts and Sciences at the Rochester Institute of Technology. In the first experiment, a

sample of alumina, referred to as the heat treated alumina sample, was placed in a kiln which was allowed to ramp up to 800°C over a period of 6 hours, held at 800°C for another 8 hours and then allowed to gradually cool to room temperature for another 6 hour period. The second experiment involved heating a sample of alumina, referred to as the quenched sample, to 1200°C, holding it at that temperature for a period of 8 hours and then quenching it in water. Each of these thermally treated samples as well as the original alumina were then evaluated using an X-ray diffraction technique. If the coordination of the alumina were to completely change to that of an amorphous state there would be an expected lowering of intensity of the peaks so that the entirety of the x-ray diffraction pattern would be encompassed by the amorphous halo [45]. As can be seen from figures 6.6-6.8, none of the heat treatments presented was capable of completely transforming the alumina to the amorphous state. Each sample still contains some trace of crystalline alumina. Due to the unavailability of proper equipment, the degree of crystallinity cannot be adequately determined for each of these samples.

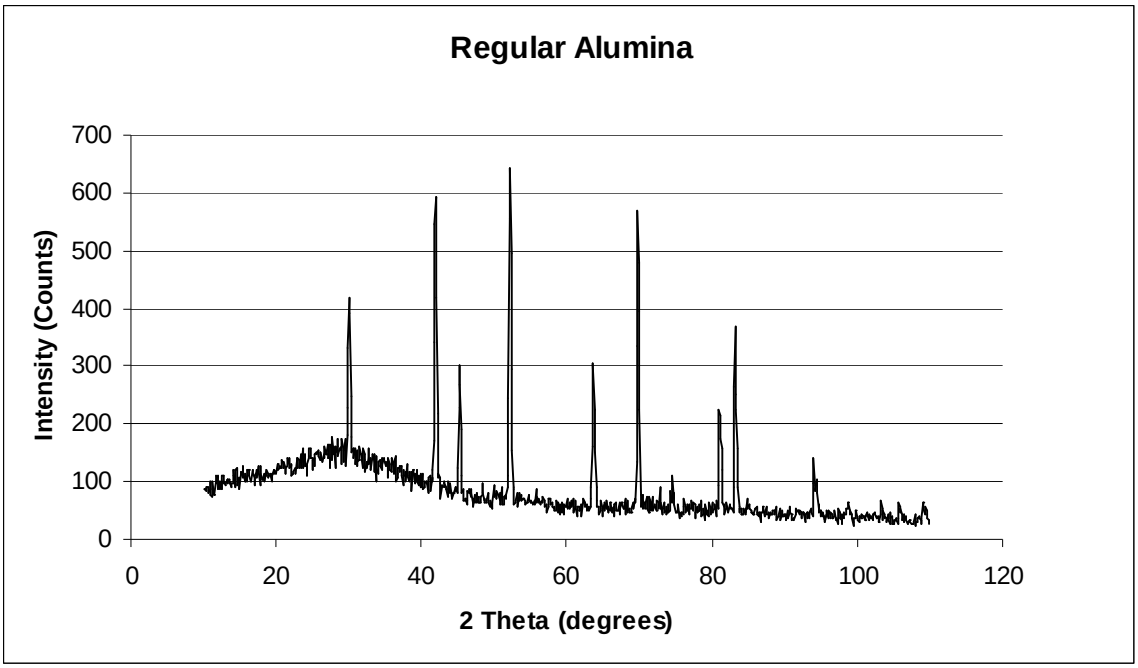

Figure B.1: X-ray diffraction spectra for the regular alumina sample.

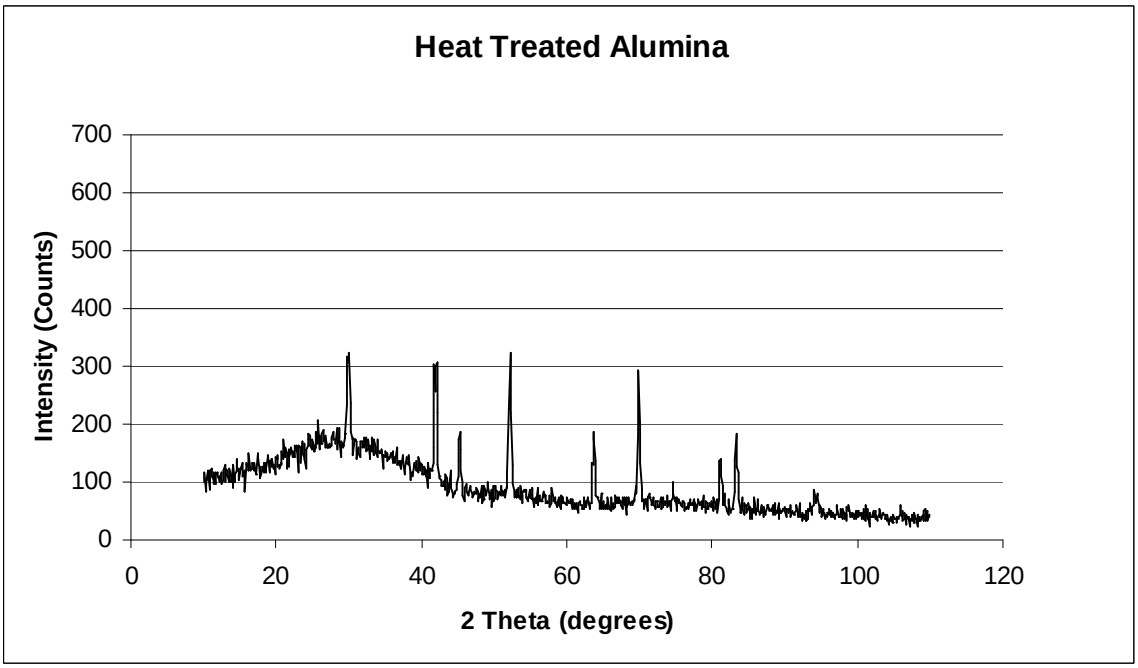

Figure B.2: X-ray diffraction spectra for the heat-treated alumina sample.

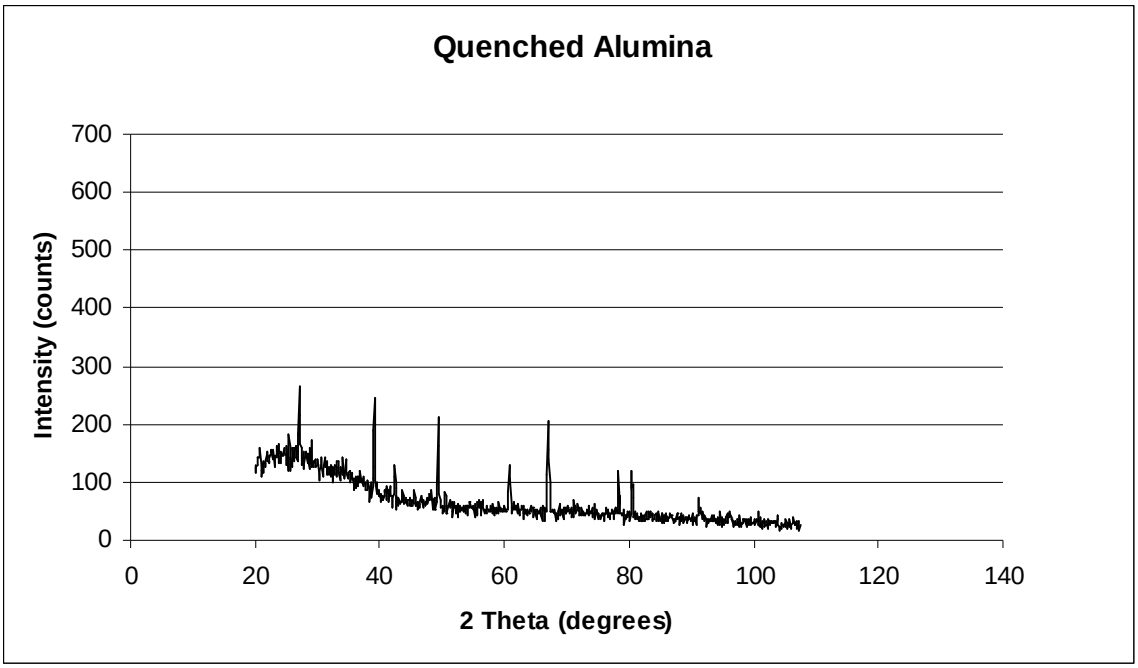

Figure B.3: X-ray diffraction spectra for the quenched alumina sample.

Appendix C: Error Determination and Propagation

Errors for percent pore volume, sample density, and both speeds of sound were determined through standard deviations. The standard deviations for the percent pore volume and density were calculated from the raw collected data; however, the speed of sound uncertainty was calculated as the standard deviation of the group velocities after converting back from the phase velocities. Error values for the elastic properties were then calculated as the addition of the relative error for each multiplied term. For example, for a function, f(AB) = A*B, the uncertainties would be given as [47]:

$$\left(\frac{\Delta f}{f}\right)^2 = \left(\frac{\Delta A}{A}\right)^2 + \left(\frac{\Delta B}{B}\right)^2 \qquad \text{(C.1)}$$

Where Δ represents the standard deviation determined for any particular measurement.

Bibliography

[1] J. Davidovits, "Geopolymers: Inorganic Polymeric New Materials," Journal of Thermal Analysis, vol. 37, pp.1633-1656, 1991.

[2] J.A. Tossell, "A Theoretical Study of the Molecular Basis of the Al Avoidance Rule and the Spectral Characteristics of the Al-O-Al Linkages," American Mieralogist, Vol. 78 pp. 911-920, 1993

[3] B. Varela, A Study on the Suitability of Geopolymers for Structural Steel Fire Prevention. Las Cruces, New Mexico: New Mexico State University, 2002

[4] Duxson, P., Provis, J., Lukey, G., van Deventer, S. J., "Structural Ordering in Geopolymers Derived from Metakaolin," In, Geopolymer : Green Chemistrty and Sustainable Development Solutions, 2005

[5] P. Duxson, "Effect of Alkali Cations on Aluminum Incorporation in Geopolymeric Gels," Industrial Engineering Chemistry Research, vol. 44, no. 4, pp. 832, 2005

[6] H. Xu, and S.J. van Deventer, "Effect of Source Materials on Geopolymerization," Industrial Engineering Chemistry Research, vol. 42, no. 8, p. 1698, 2003

[7] A.T. Pinto, E. Viera. "Optimised Conditions for the Obtaining of Metakaolin," Materials Science Forums, vol. 514-516, pp. 1536-1540, 2006.

[8] P. Duxson, G. C. Lukey, S. W. Mallicoat, W. M. Kriven, and J.S.J. van Deventer, "Understanding the Relationship between Geopolymer Composition, Microstructure and Mechanical Properties," Colloids and Surfaces. A, Physicochemical and Engineering Aspects, vol. 269, no. 1, p. 47, 2005.

[9] W.M. Kriven and J.L. Bell. "Effect of Alkali Choice on Geopolymer Properties" In Ceramic Engineering and Science Proceedings. 2004, pp. 99-104

[10] P.S. Singh, "Outstanding Problems Posed by Nonpolymeric Particulates in the Synthesis of a Well-Structured Geopolymeric Material," Cement and Concrete Research, vol. 34, no. 10, pp. 1943, 2004

[11] Sindhunata, "Effect of Curing Temperature and Silicate Concentration on Fly-Ash-Based Geopolymerization," Industrial Engineering Chemistry Research, vol. 45, no. 10, pp. 3559, 2006

[12] H. Wang, H. Li, and F. Yan, "Synthesis and Mechanical Properties of Metakaolinite-Based Geopolymer," Colloids and SurfacesA: Physicochem. Eng. Aspects, vol. 268, no. 1-3, pp. 3976-3981, 2005.

[13] L. Weng, K. Sagoe-Crentsil, T. Brown, and S. Song, "Effects of Aluminates on the Formation of Geopolymers" Materials Science and Engineering B. vol. 117, no. 2 pp.163-168, 2004.

[14] W. K. W. Lee, and J.S.J. van Deventer, "The Effects of Inorganic Salt Contamination on the Strength and Durability of Geopolymers," Colloids and Surfaces A: Physichochem. Eng. Aspects vol. 211, no. 2-3, pp. 115-126, 2002.

[15] M.D.M. Paiva, E. P. Marinho, and V. G. Oliveria, "Rheological and mechanical evaluation of geopolymer-Portland cementing systems," World Congress Geopolymers 2005, Joseph Davidovitis, ed. Institut Geopolymere, Saint-Quentin, France, pp. 123-126.

[16] N A Miller, C D Stirling, and C L Nicholson, 2005, "The relationship between cure conditions and flexural properties in flyash-based geopolymers," World Congress Geopolymer 2005, Joseph Davidovitis, ed. Institut Geopolymere, Saint-Quentin, France, pp. 121-122.

[17] P. Duxson, S.W. Mallicoat, G.C. Lukey, W.M. Kriven, and J.S.J. van Deventer. "The Effect of Alkali and Si/Al ratio on the Development of Mechanical Properties of Metakaolin-Based Geopolymers." Colloids and Surfaces A: Physicochem. Eng. Aspects, vol. 292, no. 1, pp. 8-20, 2006.

[18] Jirasit, F., Lohaus, L., "Effects of High Silica-Content Materials on Fly Ash-Based Geopolymeric Cement Properties," In, Geopolymer : Green Chemistrty and Sustainable Development Solutions, 2005

[19] J. C. Swanepoel, "Utilisation of Fly Ash in a Geopolymeric Material," Applied Geochemistry, vol. 17, no. 8, p. 1143, 2002.

[20] H. Wang, H. Li, and F. Yan, F, "Synthesis and Tribological Behavior of Metakaolinite-Based Geopolymer Composites," Materials Letters, vol. 59, no. 29-30, pp. 3976-3981, 2005.

[21] A. Teixeira-Pinto, B. Varela, K. Shrotri, R.S. Pai Panandiker, J. Lawson. "Geopolymer-Jute composite; A novel environmentally friendly composite with fire resistant properties." In 31st International Conference on Advanced Ceramics and Composites. Daytona Beach Fl. 2007

[22] J.G.S. van Jaarsveld, J.S.J. van Deventer. "The Effect of Metal Contaminants on the Formation and Properties of Waste-Based Geopolymers." Cement and Concrete Research. Vol. 29, no. 8, pp. 1189-1200, 1999.

[23] A.J. Foden, P. Balaguru, and R.E. Lyon, "Fire Response of Geopolymer Structural Composites," In Proceedings from the First International Conference on Fiber Composites in Infrastructure, 1996, pp.972-981

[24] J. Davidovits 1994. "Global Warming Impact on the Cement and Aggregates Industries," World Resource Review Vol.6 No. 2 pp. 263-278

[25] S.R. Mishra, S. Kuman, A.Park, J.Rho, J.Losby, B.K. Horrmeister, "Ultrasonic Characterization of the Curing Process of PCC Fly Ash-Cement Composites," Materials Characterization, vol. 50, no. 4-5, pp. 317-323, 2003.

[26] J.G.S. van Jaarsveld, J.S.J. van Deventer, L. Lorenzen. "The Potential Use of Geopolymeric Materials to Immobilise Toxic Metals: Part I. Theory and Applications" Minerals Engineering vol.10, no.7, pp. 659-669, 1996

[27] R.B. Thompson, "Ultrasonic measurement of mechanical properties," In IEEE Ultrasonics Symposium, 1996, pp. 735-744

[28] J. McHugh and J. Doring, "Relationship between the Mechanical and Ultrasound Properties of Polymer Materials," In *ECNDT 2006, 2006*

[29] T. L. Szabo. Diagnostic Ultrasound Imaging: Inside Out. Burlington, MA: Elsevier Academic Press, 2004.

[30] R. Halmshaw, NDT Data Fusion, New York, NY: Halsted Press, 1991

[31] Standard Practice for Measuring Ultrasonic Velocity in Materials. ASTM standard E 494-95 (Reapproved 2001)

[32] C.M. Sayers, "ULTRASONIC VELOCITY DISPERSION IN POROUS MATERIALS." Journal of Physics. D, Applied Physics, vol. 14, no. 3, pp. 413, 1981.

[33] L. Chang, "Characterization of Alumina Ceramics by Ultrasonic Testing," Materials Characterization, vol. 45, no. 3, pp. 221, 2000

[34] D. Laux, J.Y. Ferrandis, J. Bentama, M. Rguiti, "Ultrasonic Investigation of Ceramic Clay Membranes," Applied Clay Science. vol. 32, no. 1-2 pp. 82-86, 2005

[35] P. Shull and B.R. Tittmann, "Ultrasound," in *Nondestructive Evaluation: Theory, Techniques, and Applications* P. Shull, ed. Columbus, OH: CRC Press, 2002, pp63-89.

[36] J.D. Achenbach, *Wave Propagation in Elastic Solids,* New York: American Elsevier Publishing Company, 1973.

[37] Marczak, Wojciech, "Water as a Standard in the Measurements of Speed of Sound in Liquids." Journal of the Acoustical Society of America, vol. 102, no. 5 , pp. 2667-2779, 1997

[38] L. Cohen, "Time-Frequency Distributions-A Review," In Proceedings of the IEEE, 1989 pp. 941-81

[39] "MetaMax Technical Bulletin," BASF Corporation, rev. 08/2006

[40] Alcoa Co. Specifications Document for Mic-6 products. http://www.alcoa.com/mill_products/north_america/en/product.asp?cat_id=1481&prod_id=619

[41] P.M. Ossi, Disordered Materials: An Introduction. Berlin, Germany: Springer, 2006

[42] C. Banwell, Fundamentals of Molecular Spectroscopy. Berkshire, England: McGraw Hill, 1966

[43] Lee, W.K.W., van Deventer, J.S.J., 2002, "Effects of Anions on the Formation of Aluminosilicate Gel in Geopolymers," Ind. Eng. Chem. Res. 41, 4550-4558

[44] *The Infrared Spectra of Minerals* Farmer, V.C., ed. London: Mineralogical Society 1974.

[45] Godbar, J., Ozin, G.A., 1988, "Fourier Transform Far-Infrared Spectroscopic Study of Cation and Anion Dynamics in M,X-Sodalites, Where M = Li', Na', K', Rb', Ca2'; X = CI-, Br-, I-, C104-, OH," Journal of Physical Chemistry, 92, 4980-4987

[46] Lee, W.K.W., vanDeventer, 2003, "Use of Infrared Spectroscopy to Study Geopolymerization of Heterogeneous Amprphous Aluminosilicates" Langmuir, 19, pp. 8726-8734

[47] Goodman, L., "On the Exact Variance of Products," Journal of the American Statistical Society, vol. 292, no. 55, pp. 708-713 (1960)